



Master thesis
Master of Science
Computer Engineering

PERFORMANCE OF PROCESSING-NODE
REPEATERS WITH TIME-MULTIPLEXED
ENTANGLEMENT GENERATION

Yu Miyawaki

July 2022

Daily Supervisor
Francisco Ferreira da Silva

Supervisor
Stephanie Wehner

ABSTRACT

Entanglement is an essential resource for a variety of applications, such as distributed quantum computing and quantum cryptography. However, long-distance entanglement generation is challenging because of two reasons: photon loss occurs as an exponential function of distance through an optical fiber and the no-cloning theorem prevent us from directly amplifying the photons. Therefore, quantum repeaters that enable long-distance communication to realize quantum information-based protocols are desired. One way to achieve a higher entanglement generation rate is to make many attempts of generating entangled states in parallel, a process known as time-multiplexing. There has been previous work investigating the performance of time-multiplexed entanglement generation using processing nodes, but only at the elementary link level. Furthermore, this analysis was restricted to the rate of entanglement generation, with no concern for the fidelity. In this work, we go further by investigating both the fidelity and the rate of entanglement generation of time-multiplexed protocols by analyzing the secret key rate (SKR) of quantum key distribution. Moreover, we also study setups with one and two repeaters. Specifically, we investigate the impact of different hardware parameters on the SKR. Among other results, we conclude that swap gate time is a key factor for achieving higher SKR. We also examine what effect different repeater-chain protocols have on the performance of repeater chains with limited hardware resources. We find that having the repeater send photons in alternating fashion towards both end nodes results in a higher SKR than generating entanglement sequentially. Besides, we investigate what is the most efficient distribution of communication qubit (CQ) in a protocol with multiple repeaters. We ascertain that the repeater chain setup in which the number of CQs in a node is equal to that node's number of neighbors makes best use of its resources.

ACKNOWLEDGEMENTS

I wish to thank Prof. Stephanie Wehner for giving me the opportunity to dedicate to the project and for all the comments.

I also would like to appreciate my daily supervisor, Francisco, for the every feedbacks on my research, the thesis, and discussions about our research. Without you, my master thesis project would have been even more difficult. Besides, thank you for reminding me that the quantum Internet requires collaboration not only with researchers in software, but also with those who have extensive knowledge about hardware field.

For all my college, David, Guus, Emlyn, Janice, and Hana, I would like to express my appreciation. I received various Inspirations from a slightly different field of my research, which made me rereconsider the direction of my own research.

I also thank Helena, the management assistant in our laboratory, for acting as a bridge between me and Stephanie and setting up meetings smoothly.

The project was a battle against many things. At the beginning of the project, the influence of COVID-19 remained strong and there were many online meetings. For an international student like me, who came to the Netherlands alone from the edge of Asia, it was a battle against loneliness. Once the COVID-19 settled down, I also suffered from light depression by the dark Dutch winter. Then, I found out my wife was pregnant and temporarily returned to Japan to support her morning sickness. Furthermore, the war by Russia has deeply troubled me with the question of what I should do in addition to what I want to do.

Under such a situation, my wife in Japan, lovely cat (Haru), our baby, and my parents have encouraged me. Thank you for healing my various stresses in a foreign country with your many smiles.

And I am sure that Ramen, Sushi and other dishes I ate when I returned to Japan have surely contribute to thousands of words in my thesis. I am grateful for such a wonderful Japanese food culture.

Finally, I would like to thank all the researchers involved in the quantum Internet. I am very happy to have had a glimpse of an interesting future standing on the shoulders of giants of research results that they have left.

CONTENTS

1	INTRODUCTION	3
2	BACKGROUND	7
2.1	Basic concepts	7
2.2	Fidelity	10
2.3	Quantum Channels and Operations with noise	11
2.4	No-cloning theorem	12
2.5	Quantum Key Distribution	13
2.5.1	BB84	13
2.5.2	Secret Key Rate	14
3	REPEATER CHAIN	15
3.1	Introduction	15
3.2	Entanglement generation protocol	15
3.2.1	Extreme-photon-loss protocol	17
3.2.2	Barrett-Kok protocol	19
3.3	Time-multiplexed entanglement generation	20
3.4	Entanglement swap	20
3.5	Quantum Repeater Hardware Platform	22
4	EFFECT OF HARDWARE IMPERFECTIONS ON SKR	25
4.1	Models	25
4.1.1	Common settings	25
4.1.2	For which parameter regimes does time-multiplexing allow for getting higher SKR than without multiplexing?	31
4.1.3	Which hardware parameters are most important for improving SKR?	31
4.1.4	What is the impact of the number of CQs on the SKR?	31
4.2	Results	32
4.2.1	For which parameter regimes does time-multiplexing allow for getting higher SKR than without multiplexing?	32
4.2.2	Which hardware parameters are most important for improving SKR?	33
4.2.3	What is the impact of the number of CQs on the SKR?	33
4.3	Summary	35
5	EFFECT OF PROTOCOL CHOICE IN SKR ACHIEVABLE BY REPEATER CHAINS WITH LIMITED RESOURCES	37
5.1	Models	37
5.1.1	Common settings	37
5.1.2	What is the best order in which to perform entanglement generation attempts?	37
5.1.3	How is the best way to distribute CQs in a chain with two repeaters?	40
5.2	Results	45
5.2.1	What is the best order in which to perform entanglement generation attempts?	45
5.2.2	How is the best way to distribute CQs in a chain with two repeaters?	46
5.3	Summary	46
6	CONCLUSION	47
6.1	Summary	47
6.2	Future work	48

1

INTRODUCTION

Entanglement is an essential resource for a variety of applications, such as distributed quantum computing [Cirac et al., 1999] and quantum cryptography [Jennewein et al., 2000]. Distributed quantum computation, a model in which components of a software system are shared among multiple quantum computers, is expected as a way of creating fault tolerant quantum computers with a few million qubits [Cuomo et al., 2020]. Quantum cryptography is a cryptographic technology that aims to provide secure communications by utilizing the properties of quantum mechanics. Quantum cryptography technology is essential because the rise of quantum computers is expected to make it easier to break the RSA cryptosystem, which is the foundation of current internet security. One of the applications of quantum cryptography is the quantum key distribution (QKD) protocol [Bennett and Brassard, 1984]. This is the protocol that uses quantum mechanics to share random secret keys. Through QKD, we can achieve secure communication between two communicating parties. In general, the higher the entanglement generation is, the faster we can execute any application we might want to use. Therefore, it is necessary to achieve a high entanglement generation rate between long-distance nodes.

However, achieving long-distance entanglement generation is challenging because photon loss occurs as an exponential function of distance when a photon passes through an optical fiber [Bouwmeester and Zeilinger, 2000]. Besides, non-orthogonal quantum states cannot be amplified like classical states due to the no-cloning theorem [Wootters and Zurek, 1982].

Therefore, a quantum repeater is desired. These are intermediate nodes between two end-nodes that may enable long-distance quantum communication. Several physical systems are being investigated as possible hardware platforms for quantum repeaters. Due to the advance stage of development of Nitrogen-vacancy (NV) center experiments, repeaters based on NV center might be feasible in the short term [Rozpdek et al., 2019]. In fact, a three-node entanglement-based NV center quantum network has recently been realized [Pompili et al., 2021]. Even though Matteo and Sophie's 3-node network experiment is extremely impressive, it was done at a very small scale. Scaling up to real-world distances will require large improvements in entanglement generation rate.

One way to achieve a higher entanglement generation rate is to make many attempts of generating entangled states in parallel, which is called time-multiplexing protocol. In the protocol, a quantum state in a communication qubit (CQ), which can emit an entangled photon, entangled with the photon is swapped with a memory qubit (MQ), which is good at keeping quantum states, after it emits the photon. Therefore, the communication qubit can send another photon soon, and repeating this process enables us to attempt to send photons in parallel. Hence, it allows higher entanglement generation.

There are several reasons for this low rate. At first, Suzanne van Dam et al. found that the bottleneck to improving the entanglement rate is the swap gate time when using the time-multiplexing protocol [Collins et al., 2007] explained in Section 3.3. However, no studies have yet reported that this value can be improved sufficiently. In addition, since the number of available communication qubits is limited to one in an NV center, we have to wait for the time until the swap gate is completed for

the next attempt and that make attempts of sending an entangled photon in parallel impossible. This also leads to a low entanglement generation rate. Therefore, it is necessary to put aside the perspective of feasibility and consider cases when changing various hardware parameters or using the other platforms with an emphasis on achieving a higher entanglement rate.

Besides, only elementary links were considered in the research by Suzanne et al. [Dam et al., 2017]. However, generating entanglement over long distances will likely require the use of multiple repeaters. It is then important to study what effect different repeater-chain protocols have on the performance of repeater chains with limited hardware resources.

Finally, in addition to the rate of quantum entanglement generation, it is significant to evaluate fidelity at the same time. The fidelity is a measure of the quality of the state, and if it's too low the entanglement is actually not usable. In an application, secret key rate (SKR), the amount of key generated per unit of time, is defined as important metric which reflects the entanglement generation rate and the fidelity. There are many studies that evaluate only rates of quantum entanglement generation with fidelity above a certain value [Pfister et al., 2016]. Hence, the major contributions of this thesis are:

- Analyzing impact of different hardware parameters on both entanglement generation rate and fidelity in an elementary link when we change some hardware parameters. To do so, we use the BB84 secret key rate (SKR) as the metric, because it is influenced by both rate and fidelity. Hence, we will conduct the research to obtain suggestions on what parameters are also key for improving it.
- Analyzing the SKR with a chain with 1 or 2 repeaters when we change repeater chain protocol or the resources in the repeaters. The evaluation can make us evaluate protocols more accurately allowing us to find more realistic protocols for QKD. This is a novel approach as previous research discussed only entanglement rate keeping a fidelity above a certain value.

Outline

This thesis is structured to guide the reader from the basic elements of the quantum mechanical theory to the final results acquired.

At first, in [Chapter 2](#) we introduce the basics of quantum mechanics needed to understand our project. In [Section 2.1](#), general information about quantum mechanics is explained. Then, fidelity to evaluate a quality for quantum states is introduced in [Section 2.2](#). In [Section 2.3](#), the noise model we use in the thesis is shown. No-cloning theorem, which is the key to understanding the motivation for quantum repeaters, is given in [Section 2.4](#). Finally, [Section 2.5](#) introduces the secret key rate, which is influenced by both the fidelity and the rate, to reflect on both the fidelity and the entanglement generation rate in the BB84 protocol.

[Chapter 3](#) discusses how to share high-quality entangled states between two parties. In [Section 3.1](#), the necessity of the quantum repeaters is explained. It is shown that there are several protocols to generate entanglement between the two quantum nodes in [Section 3.2](#). Time multiplexing entanglement is introduced in [Section 3.3](#). In [Section 3.4](#), the entanglement swap, which can be used to extend the distance spanned by entanglement, is introduced. Finally, two types of hardware platforms to realize the quantum repeaters will be introduced in [Section 3.5](#).

[Chapter 4](#) and [Chapter 5](#) start with the introduction of the research questions that will be investigated, followed by the setups under study and the results obtained. [Chapter 4](#) concerns itself with effects on SKR by changing some hardware parameters. [Chapter 5](#) investigate how repeater chain which has limited resources affects SKR and how to optimally distribute the resources to obtain larger SKR in setups consisting of two end nodes connected by up to two repeaters.

The thesis concludes in [Chapter 6](#) with a summary of our research results and some suggestions for future work.

2 | BACKGROUND

In this section, we will go through the basics of quantum mechanics needed to understand our project. The introduction given here is brief. For a more detailed exposition, see [Chuang and I.L., 2011].

2.1 BASIC CONCEPTS

Hilbert space

A quantum state is described by an element $|\psi\rangle \in \mathcal{H}$ of a complex Hilbert space, a complex linear space where the inner product is defined and completeness is guaranteed. For a finite-dimensional complex Hilbert space, $|\psi\rangle$ can be expressed as a complex column vector $(c_1, \dots, c_d)^T$. Elements on the dual space \mathcal{H} are described as $\langle\psi|$ and the inner product with $|\phi\rangle$ is depicted as $\langle\psi|\phi\rangle$. The elements on the dual space can be expressed as the complex row vector $\langle\psi| = (c_1^*, \dots, c_d^*)$. Thus, the description of a Hilbert space and its dual space using $|\rangle$ (ket) and $\langle|$ (bra) is called Dirac's bra-ket notation.

The smallest unit of information in classical information is the bit, a variable with two values, 0 and 1. Similarly, the smallest unit of quantum information is the qubit, a state in a two-dimensional complex Hilbert space. A qubit can be written in general as a linear sum of two orthogonal states ($|0\rangle$ and $|1\rangle$, which we will call the computational basis) as shown in Equation 2.1.

$$|\psi\rangle = \alpha|0\rangle + \beta|1\rangle \quad (2.1)$$

α and β are complex numbers satisfying $|\alpha|^2 + |\beta|^2 = 1$. Any two orthogonal quantum states, such as the two energy states of an atom, the orthogonal polarization states of a photon, or electron and nuclear spin can be the two orthogonal states of $|0\rangle$ and $|1\rangle$. These complex numbers can be written using $\theta \in [0, 2\pi)$ and $\phi \in [0, \pi/2)$ as shown in Equation 2.2.

$$\alpha = \cos \frac{\theta}{2}, \quad \beta = e^{i\phi} \sin \frac{\theta}{2} \quad (2.2)$$

Using these θ and ϕ , the state of a qubit can be represented on a sphere of radius 1 (Bloch sphere) as shown in Figure 2.1.

In order to study n interacting quantum systems, we must consider composite quantum systems. The quantum state of a composite system can be written as elements of a Hilbert space $\mathcal{H}_{1,2,\dots,n}$ such as $\mathcal{H}_1 \otimes \dots \otimes \mathcal{H}_n$ which is called the tensor product. When we have two vectors, $[x_0, x_1]$ and $[y_0, y_1]$, the tensor product can be calculated as shown in Equation 2.3.

$$\begin{bmatrix} x_0 \\ x_1 \end{bmatrix} \otimes \begin{bmatrix} y_0 \\ y_1 \end{bmatrix} = \begin{bmatrix} x_0 \begin{bmatrix} y_0 \\ y_1 \end{bmatrix} \\ x_1 \begin{bmatrix} y_0 \\ y_1 \end{bmatrix} \end{bmatrix} = \begin{bmatrix} x_0 y_0 \\ x_0 y_1 \\ x_1 y_0 \\ x_1 y_1 \end{bmatrix} \quad (2.3)$$

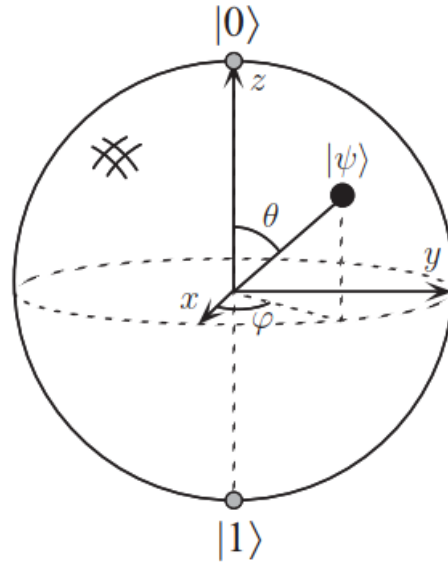


Figure 2.1: The Bloch sphere is a visualization of a single-qubit quantum state on a 3-dimensional sphere. For example, if the quantum state $|\psi\rangle$ is $|0\rangle$, it is represented on the Bloch sphere by the vector in the positive direction on the z axis. If the state is $|+\rangle = \frac{1}{\sqrt{2}}(|0\rangle + |1\rangle)$, it is represented by the vector in the positive direction on the x -axis.

For example, the product state of $|\psi\rangle_1 \in \mathcal{H}_1$ and $|\phi\rangle_2 \in \mathcal{H}_2$, $|\psi\rangle_1 \otimes |\phi\rangle_2$, is in a composite system consisting of two quantum systems. Composition of quantum systems is linear, therefore the linear sum of the two product states of $|\psi\rangle_1 \otimes |\phi\rangle_2$ and $|\psi'\rangle_1 \otimes |\phi'\rangle_2$ is also contained in the composite system $\mathcal{H}_{1,2}$. Thus, the linear space spanned by the product states of elements of \mathcal{H}_1 and \mathcal{H}_2 is $\mathcal{H}_{1,2} = \mathcal{H}_1 \otimes \mathcal{H}_2$. Similarly, the Hilbert space of a composite system consisting of n quantum systems can be written as $\mathcal{H}_1 \otimes \cdots \otimes \mathcal{H}_n$. The computational basis in the space with 2^n elements is spanned by the vectors $\mathcal{C}_n = \{|j\rangle \mid j \in \{0,1\}^n\}$, where $\{0,1\}^n$ is the space of all the combinations of n 0 and 1. However, not all states can be written as tensor products. In particular, the states that can be written like this are product states, while the states that cannot are called entangled states. Well-known examples of two-qubit entangled states are the Bell states, shown in [Equation 2.4](#).

$$\begin{aligned}
 |\Phi_+\rangle &= \frac{1}{\sqrt{2}}[|00\rangle + |11\rangle] \\
 |\Psi_+\rangle &= \frac{1}{\sqrt{2}}[|01\rangle + |10\rangle] \\
 |\Phi_-\rangle &= \frac{1}{\sqrt{2}}[|00\rangle - |11\rangle] \\
 |\Psi_-\rangle &= \frac{1}{\sqrt{2}}[|01\rangle - |10\rangle]
 \end{aligned} \tag{2.4}$$

Time-evolution of closed quantum systems

The time evolution of a closed quantum system, i.e., a system which does not interact with its environment, is represented by the Schrödinger equation using a Hermitian operator, H , as shown in [Equation 2.5](#).

$$i\hbar \frac{\partial}{\partial t} |\psi(x,t)\rangle = H |\psi(x,t)\rangle \tag{2.5}$$

Given a state $|\psi(x,0)\rangle$ at time $t = 0$, we can solve the Schrödinger equation as

shown in [Equation 2.6](#).

$$|\psi(x, t)\rangle = e^{-iHt/\hbar}|\psi(x, 0)\rangle \quad (2.6)$$

Since H is a Hermitian operator, $U = e^{-iHt/\hbar}$ is a unitary operator satisfying $U^\dagger U = I$. Thus, the time evolution of a quantum system is described by the unitary operator U acting in the complex Hilbert space.

Measurement for pure states

[Equation 2.5](#) holds only for closed quantum systems. Interactions between a quantum system and outside the world, such as a measurement, cannot be described by a unitary operator. Measurement of a quantum system can be described by a projective measurement with a projection operator $\{P_i\}_{i=1}^d$. Projection operators are a set of Hermitian operators satisfying $P_i P_j = \delta_{ij} P_i$ and $\sum_{i=1}^d P_i = I$. For a state $|\psi\rangle$, the probability p_i of obtaining the measurement result i when performing a projective measurement with the projection operator $\{P_i\}$ can be calculated as shown in [Equation 2.7](#).

$$p_i = \|P_i|\psi\rangle\|^2 = \langle\psi|P_i|\psi\rangle \quad (2.7)$$

It follows that $\sum_i p_i = 1$. The post-measurement state after getting the measurement result i is $P_i|\psi\rangle/\sqrt{p_i}$.

Measurement for mixed states

In the above, we have considered situations where one quantum state $|\psi\rangle$ is given with probability 1. However, a qubit that is initially a pure state $|\psi\rangle$ may become mixed, since external noise occurs due to undesired interactions with the environment. Therefore, we need to extend this to consider cases where different quantum states with some probabilities are given. To consider this, it is convenient to describe the quantum state using the density operator $\rho = |\psi\rangle\langle\psi|$. The probability of the projective measurement with the projection operator $\{P_k\}$ can be computed as in [Equation 2.8](#) using the trace, $\text{Tr}[\dots] = \sum_{i=1}^d \langle i|\dots|i\rangle$. The completeness ($\sum_i |i\rangle\langle i| = I$) of the orthonormal basis ($\{|i\rangle\}_{i=1}^d$) is used. And, it satisfies $\text{Tr}[ABC] = \text{Tr}[CAB]$. Assuming different quantum states $\{|\psi_j\rangle\}$ with probability $\{q_j\}$, the projective measurement $\{P_i\}$ is performed. Using the joint law of probability, the probability of obtaining the measurement result i is as shown in [Equation 2.8](#).

$$p_i = \sum_j q_j \text{Tr}[P_i|\psi_j\rangle\langle\psi_j|] = \text{Tr}\left[P_i \sum_j q_j |\psi_j\rangle\langle\psi_j|\right] \quad (2.8)$$

Therefore, using $\rho \equiv \sum_j q_j |\psi_j\rangle\langle\psi_j|$ as the density operator, the probability distribution of the projective measurement for such a stochastic mixed state is given by $\text{Tr}[P_i\rho]$. To let $\sum_i p_i = 1$ hold, $\text{Tr}[\rho] = 1$ is required.

Quantum gates

Quantum gates are linear and unitary. That is, all operations are linear transformations of states. Besides, unitarity means that $U^\dagger U = U U^\dagger = I$ for any quantum gate U , with I being the identity matrix.

The Pauli matrices, together with the identity matrix, constitute a basis for all single-

qubit quantum gates as shown in Equation 2.9.

$$I = \begin{pmatrix} 1 & 0 \\ 0 & 1 \end{pmatrix}, \quad X = \begin{pmatrix} 0 & 1 \\ 1 & 0 \end{pmatrix}, \quad Y = \begin{pmatrix} 0 & -i \\ i & 0 \end{pmatrix}, \quad Z = \begin{pmatrix} 1 & 0 \\ 0 & -1 \end{pmatrix} \quad (2.9)$$

I_n is the identity matrix of dimension n . The identity matrix in Equation 2.9 should then be denoted as I_2 for consistency.

X corresponds to the classical bit inversion (NOT) and its effect on the computational basis states is shown in Equation 2.10.

$$X|0\rangle = |1\rangle, \quad X|1\rangle = |0\rangle \quad (2.10)$$

Z acts like Equation 2.11, and corresponds to reversing the phases of $|0\rangle$ and $|1\rangle$.

$$Z|0\rangle = |0\rangle, \quad Z|1\rangle = -|1\rangle \quad (2.11)$$

The Y operator can be written as $Y = iXZ$, combining phase inversion and bit inversion.

One other important operator is the Hadamard gate as shown in Equation 2.12. This operator transforms one Pauli basis into another. In other words, the Hadamard gate corresponds to the interchange of the x-axis and z-axis on the Bloch sphere.

$$H = \frac{1}{\sqrt{2}} \begin{pmatrix} 1 & 1 \\ 1 & -1 \end{pmatrix} \quad (2.12)$$

To perform operations on arbitrary n qubits, two-qubit interactive operations are needed. The typical two-qubit operation is controlled-not (CNOT) gate as shown in Equation 2.13. The CNOT gate flips the target qubit when the state of the control qubit is $|1\rangle$. Furthermore, the CNOT gate, the Hadamard gate, and the Pauli gates constitutes a universal gate set which is finite set of gates that can approximate any unitary matrix arbitrarily well [Chuang and I.L., 2011].

$$H = \begin{pmatrix} I & O \\ O & X \end{pmatrix} = \begin{pmatrix} 1 & 0 & 0 & 0 \\ 0 & 1 & 0 & 0 \\ 0 & 0 & 0 & 1 \\ 0 & 0 & 1 & 0 \end{pmatrix} \quad (2.13)$$

2.2 FIDELITY

Quantum states often deviate from their expected state due to noise. It is then useful to quantify this deviation, which corresponds to the distance between two quantum states. Commonly used indicators are fidelity and trace distance. The fidelity of states ρ and σ is defined as Equation 2.14 [Jozsa, 1994]. It takes values from 0 to 1. It is 1 if the states are equal, and 0 if they are orthogonal.

$$F(\rho, \sigma) = \left(\text{tr} \left[\sqrt{\sqrt{\rho}\sigma\sqrt{\rho}} \right] \right)^2 \quad (2.14)$$

This expression can be simplified in some situations: the first is when ρ and σ commute and the second is when comparing the fidelity between a pure state $|\psi\rangle$ and an arbitrary mixed state ρ .

When ρ and σ commute, i.e. $\rho\sigma - \sigma\rho = 0$ holds, they are diagonal in the same basis for some orthonormal basis $|i\rangle$. In other words, $\rho = \sum_i a_i |i\rangle\langle i|$, $\sigma = \sum_i b_i |i\rangle\langle i|$. In this special case, we can think $F(\rho, \sigma)$ as a classical fidelity $F(a_i, b_i)$ between the eigenvalues a_i and b_i (Equation 2.15).

$$\begin{aligned} F(\rho, \sigma) &= \left(\text{tr} \left[\sqrt{\sum_i a_i b_i |i\rangle\langle i|} \right] \right)^2 \\ &= \sum_i a_i b_i \\ &= F(a_i, b_i) \end{aligned} \quad (2.15)$$

Fidelity is also easily expressed when comparing a pure state $|\psi\rangle$ and an arbitrary mixed state ρ . By expanding Equation 2.14, we get the expression similar to Equation 2.7 like Equation 2.16. In other words, this can be thought of as a kind of probability of measuring $|\psi\rangle$ from ρ . If ρ is also a pure state $|\phi\rangle$, then $F(|\psi\rangle, |\phi\rangle)$ can be expressed as $\langle\psi|\phi\rangle$.

$$\begin{aligned} F(|\psi\rangle, \rho) &= \left(\text{tr} \left[\sqrt{\langle\psi|\rho|\psi\rangle} |\psi\rangle\langle\psi| \right] \right)^2 \\ &= \langle\psi|\rho|\psi\rangle \end{aligned} \quad (2.16)$$

2.3 QUANTUM CHANNELS AND OPERATIONS WITH NOISE

Although the time evolution of a closed system is described by unitary transformations, the same is not true for open quantum systems. Open quantum systems are systems that interact with their environment. Their evolution is generally expressed by non-unitary transformations. There are three main ways to describe the quantum state of the system apart from the environment in such cases: partial tracing of environment, the Kraus operators formalism and completely positive trace preserving (CPTP) maps. Since these representations are equivalent to each other, we only discuss the Kraus representation.

We start by describing the partial trace operation, since it is of general interest. When the density operator of the system of interest (S) is ρ_s and the initial state of the environment (E) is $|0\rangle_E \langle 0|_E$, the entire quantum state can be described by $\rho_s \otimes |0\rangle_E \langle 0|_E$. Since this is the closed system, the time evolution is described by unitary transformation on the joint system of the state and environment. In other words, when we consider interactions such as noise, the entire system can be described as Equation 2.17 using a certain unitary transformation U .

$$\rho_s \otimes |0\rangle_E \langle 0|_E \rightarrow U (\rho_s \otimes |0\rangle_E \langle 0|_E) U^\dagger \quad (2.17)$$

In this case, the time evolution of the system of interest can be described by taking a partial trace of the environmental system as shown in Equation 2.18.

$$\begin{aligned} \Gamma(\rho_s) &= \text{Tr}_E \{ U (\rho_s \otimes |0\rangle_E \langle 0|_E) U^\dagger \} \\ &= \sum_j \langle j|_E U (\rho_s \otimes |0\rangle_E \langle 0|_E) U^\dagger |j\rangle_E \\ &= \sum_j \langle j|_E U |0\rangle_E \rho_s \langle 0|_E U^\dagger |j\rangle_E \\ &= \sum_j M_j \rho_s M_j^\dagger \end{aligned} \quad (2.18)$$

$M_j \equiv \langle j|_E U | 0 \rangle_E$ is called the Kraus operator, and the last expression in [Equation 2.18](#) is called the Kraus expression.

One of the environmental effects is depolarizing noise. The depolarizing noise is a non-dissipative channel and a single state affected by the noise can be expressed by [Equation 2.19](#). This represents that the single state ρ before being affected by noise will be the fully mixed state $I/2$, the state where all the information is removed, with probability p . This is widely used as a worst case scenario approach to model noise [[Chuang and I.L., 2011](#)].

$$\Gamma(\rho) = p \frac{I}{2} + (1-p)\rho \quad (2.19)$$

This expression can be derived from the [Equation 2.18](#) assuming $M_0 = \sqrt{1-q}I$, $M_1 = \sqrt{\frac{q}{3}}X$, $M_2 = \sqrt{\frac{q}{3}}Y$, $M_3 = \sqrt{\frac{q}{3}}Z$ and using the identity related to density operations ($\Gamma(\rho) = (1-q)\rho + \frac{q}{3}(X\rho X + Y\rho Y + Z\rho Z)$, $q = 3p/4$) as [Equation 2.20](#).

$$\begin{aligned} \Gamma(\rho) &= \sum_j M_j \rho M_j^\dagger \\ &= (1-q)\rho + \frac{q}{3} (X\rho X^\dagger + Y\rho Y^\dagger + Z\rho Z^\dagger) \\ &= \frac{2q}{3}I + (1 - \frac{4q}{3})\rho \\ &= p \frac{I}{2} + (1-p)\rho \end{aligned} \quad (2.20)$$

2.4 NO-CLONING THEOREM

The no-cloning theorem states that it is impossible to make perfect copies of non-orthogonal states [[Wootters and Zurek, 1982](#)]. It is at the basis of several quantum information security properties. For example, the security of the BB84 protocol introduced in [Section 2.5](#) is based on this theorem. Intuitively, it makes eavesdropping impossible because the eavesdropper cannot learn anything about the state without disturbing it. On the other hand, the theorem makes it impossible to convey information over long distances as done classically, i.e., through amplification.

There are several ways to prove the no-cloning theorem. For example, it can be proven by showing that assuming that there is a quantum gate that clones a state leads to a contradiction.

First, cloning a state $|\psi\rangle$ can be expressed by [Equation 2.21](#).

$$|\psi\rangle \longrightarrow |\psi\rangle|\psi\rangle \quad (2.21)$$

This equation must hold for any quantum state, so [Equation 2.22](#) should also be true for ϕ different than ψ .

$$|\phi\rangle \longrightarrow |\phi\rangle|\phi\rangle \quad (2.22)$$

Assuming linearity in clone, the clone of a linear combination of the left-hand side of the two equations above must be a linear combination of the right-hand side as shown in Equation 2.23.

$$a|\psi\rangle + b|\phi\rangle \longrightarrow a|\psi\rangle|\psi\rangle + b|\phi\rangle|\phi\rangle \quad (2.23)$$

On the other hand, if we consider $|s\rangle = a|\psi\rangle + b|\phi\rangle$ as one state and clone it, Equation 2.24 should hold.

$$|s\rangle \longrightarrow |s\rangle|s\rangle = a^2|\psi\rangle|\psi\rangle + b^2|\phi\rangle|\phi\rangle + ab|\phi\rangle|\psi\rangle + ab|\psi\rangle|\phi\rangle \quad (2.24)$$

However, since $|s\rangle|s\rangle \neq a|\psi\rangle|\psi\rangle + b|\phi\rangle|\phi\rangle$, the clone is not possible. Therefore, no-cloning theorem holds.

2.5 QUANTUM KEY DISTRIBUTION

It has been suggested that the 2048-bit RSA algorithm, which is in common use today, could be deciphered by a large-scale quantum computer, which could be put into practical use around 2030 [Lily Chen, 2016]. For example, it has been shown that a quantum computer with 20 million noisy qubits can factor 2048-bit integers in 8 hours [Gidney and Ekerå, 2021]. A possible solution lies in quantum key distribution (QKD), which is a protocol in which two parties share random secret keys, is a provably secure communication method. By using the key generated through QKD to, for example, perform one-time pad (OTP), secure communication can be achieved. BB84 [Bennett and Brassard, 1984] is an original example of QKD proposed by H. Bennett et al. in 1984. Since it was first proposed in 1984, great strides have been made. More recently, in 2018, H.Yuen et al. implemented a variant protocol of the BB84 and achieved a secret key rate of over 10 Mb/s [Yuan et al., 2018]. Besides, we can buy QKD system such as Clavis XG QKD System produced by ID Quantique, Inc.. Since it has attracted great social attention, BB84 is used in our thesis as the application of entanglement generation.

2.5.1 BB84

Originally, single-photon sources are used in the BB84 protocol, and quantum entanglement generation sources are used in the other QKD protocols such as E91 [Ekert, 1992]. We assume the entanglement-based version of BB84 protocol such as E91. The entanglement-based BB84 protocol is implemented by the following steps.

Entanglement-based BB84 protocol

(step 1) Alice and Bob share entangled states.

(step 2) Alice and Bob measure the photons in a basis from X or Z basis.

(step 3) Alice and Bob exchange the bases with each other through the classical channel, and the keys in the rounds in which the measurement is performed using a different basis are discarded.

(step 4) To consider eavesdroppers, they sacrifice m bits to estimate their average correlation. If the error rate is lower than 15%, the remaining bits constitute the raw key [Branciard et al., 2005]. If not, the key is discarded.

2.5.2 Secret Key Rate

When performing entanglement-based QKD, secret key rate (SKR), the amount of key generated per unit of time, is an important metric and can be calculated as secret key fraction (SKF) \times entanglement generation rate. The SKF represents what fraction of the entangled states shared between them is available as keys and can be calculated as in Equation 2.25. The quantum bit error rate in the $Z(X)$ basis, $Q_Z(Q_X)$, is the probability that Alice and Bob get different outcomes when they both measure their systems in the basis $Z(X)$. $h(x)$ is the binary entropy function which represents the average amount of information (entropy) when an event occurs. In other words, in Equation 2.25, we deduct the amount of useless information as a key obtained when measuring quantum states in the X or Z basis in the entanglement-based BB84 protocol described above from the total.

$$SKF = 1 - h(Q_X) - h(Q_Z), h(x) = -x \log x - (1 - x) \log(1 - x) \quad (2.25)$$

SKR reflects both the fidelity and the entanglement generation rate. Therefore, in this thesis, we adopt SKR as an important metric to evaluate various entanglement generation protocols.

3

REPEATER CHAIN

In this chapter, we specifically discuss how to share high quality entangled states between two distant parties. As mentioned in [Chapter 1](#), quantum repeaters are necessary because photon loss grows exponentially with distance. Protocols for entangling neighboring quantum nodes that can generate light-matter entanglement are introduced in [Section 3.2](#). Time multiplexing entanglement [Section 3.3](#) is a way to create quantum entanglement in these protocols more efficiently. Entanglement between these two nodes is then swapped [Section 3.4](#) to expand the distance at which entanglement can be established. By performing this operation with an efficient repeater chain network protocol, high quality entangled states can be shared between the two parties. Finally, in [Section 3.5](#), we introduced some physical systems that can be used to realize such entanglement generation protocols.

3.1 INTRODUCTION

In order to share end-to-end entanglement, or to send quantum information from one node to another, it is essential to have a quantum repeater with a long quantum memory. This is because the survival probability of a photon decreases exponentially with transmission distance and no-cloning theorem makes information amplification impossible. The latest research by Simon et al. shows that a typical fiber has a loss of 0.22 dB/km at a wavelength of 1550 nm, and the probability of transmission can be as low as 10^{-22} when communicating over a distance of 1000 km [[Bayliss and Hardy, 2012](#)]. Furthermore, more efficient entanglement generation protocols (e.g., time-multiplexed) require the property of long-lived memory. In [[Muralidharan et al., 2016](#)], repeaters are classified into different generations according to their level of technological development. We only consider the first generation repeater. And in our research, we look at only processing-node repeaters with the ability to measure quantum states, emit entangled photons and do entanglement swap. In first generation repeaters, loss errors are suppressed by heralded entanglement generation, and operation errors are suppressed by heralded entanglement purification that consumes two or more entangled states to create an entangled state with higher fidelity [[Horodecki et al., 1997](#)]. These conduct quantum state measurements in the process. Depending on the result of the quantum state measurement, the quantum manipulation method to obtain the correct entanglement will change. Therefore, by heralding the outcomes of measurement to each node, we can manipulate quantum states and correct entangled states are generated. The process of the heralding requires two-way communication. Finally, end-to-end entanglement is eventually generated by swapping.

3.2 ENTANGLEMENT GENERATION PROTOCOL

One of the methods to generate quantum entanglement using the processing-node repeaters is heralded entanglement generation protocol. That means that the station with photon detectors and a beam splitter between two nodes can let us know the success or failure for attempts. We consider the two heralded entanglement gen-

eration protocol: the extreme-photon-loss entanglement generation and the Barrett-Kok (double-click) [Section 3.2](#). The former performs entanglement purification in addition to single-click, which detects a single photon at the heralding station. The latter detects two photons at an heralding station. The underlying building blocks for these protocols are the single-click protocol and entanglement purification [Section 3.2](#). Therefore, we will introduce them at first, and explain about extreme-photon-loss and Barrett-Kok in [Section 3.2](#)

Single-click

In this protocol, a weakly entangled state is generated. We start by creating the following superposition state ([Equation 3.1](#)) on a matter qubit at each node. $|0\rangle$ represents the bright state, i.e., a state that decays through photon emission. α is the bright-state population which is same as the probability of photon emission.

$$|\alpha\rangle = \sqrt{\alpha}|0\rangle + \sqrt{1-\alpha}|1\rangle \quad (3.1)$$

Decay of the bright state is accompanied by photon emission, resulting in the creation of an entangled matter-light state, as seen in [Equation 3.2](#). p denotes the state of a photon and $|1\rangle$ represents presence of a photon ($|0\rangle$ represents absence of a photon). Incidentally, the matter is called communication qubit which emits photons. In addition, qubit which cannot emit photons and tends to be used for keeping quantum states is called memory qubit.

$$|\alpha, p\rangle = \sqrt{\alpha}|0\rangle|1\rangle_p + \sqrt{1-\alpha}|1\rangle|0\rangle_p \quad (3.2)$$

After the matter-light entangled state is generated, the emitted photon(s) are sent through the fiber to the heralding station which consists of a beam splitter and photon detectors.

The beam splitter at the heralding station removes information about the node from which the photon arrived. The state before going through the beam splitter is the following:

$$|\Psi_{m_A m_B p_A p_B}\rangle = \alpha|0011\rangle + \sqrt{\alpha(1-\alpha)}|0110\rangle + \sqrt{\alpha(1-\alpha)}|1001\rangle + (1-\alpha)|1100\rangle \quad (3.3)$$

After passing through the 50:50 beam splitter, the following quantum state is obtained.

$$\begin{aligned} |\Psi_{m_A m_B p_A p_B}\rangle &= (1-\alpha)|11\rangle|00\rangle \\ &+ \sqrt{\alpha(1-\alpha)}\left[\frac{1}{\sqrt{2}}(-i|01\rangle + |10\rangle)|01\rangle + \frac{1}{\sqrt{2}}(|01\rangle - i|10\rangle)|10\rangle\right] \\ &- \frac{i}{2}\alpha|00\rangle(|20\rangle + |02\rangle) \end{aligned} \quad (3.4)$$

If a single photon detector clicks, then we know that an entangled state has been created, as shown in [Equation 3.5](#). We will have a mixed state of $|\psi_-\rangle = \frac{1}{\sqrt{2}}[|01\rangle - i|10\rangle]$ (or, if the photon is detected by another photon detector, $|\psi_+\rangle = \frac{1}{\sqrt{2}}[|01\rangle + i|10\rangle]$) and $|00\rangle$.

If both nodes emit a photon and two photons are detected by the same detector, we get the state $|00\rangle$ instead of the intended entangled state. Note that we assume that the detectors are not number-resolving, i.e., they don't know if one or more photons arrive. In [Equation 3.5](#), α' equals $(2 - \frac{5\alpha}{4}) / (2 - \alpha)$. From [Equation 3.4](#), we can see that the larger α is, the more likely photon emission is. In other words, the protocol

has a higher success probability. However, from Equation 3.5, we can see that the fidelity of the entangled state obtained is small if α is large. Therefore, α is usually picked to be small so that the fidelity is high which then results in a low success probability.

$$\rho_{m_A m_B} = \alpha' |\psi_{\pm}\rangle \langle \psi_{\pm}| + (1 - \alpha') |00\rangle \langle 00| \quad (3.5)$$

More precisely, the weakly entangled state obtained by single-click is generally represented as Equation 3.6 from the effects of phase difference ϕ the state acquires as it travel through the fiber [Kalb et al., 2017]. $|\psi_{\phi}\rangle = (|01\rangle + e^{i\phi}|10\rangle) / \sqrt{2}$.

$$\rho_{m_A m_B} = \alpha' |\psi_{\phi}\rangle \langle \psi_{\phi}| + (1 - \alpha') |00\rangle \langle 00| \quad (3.6)$$

Entanglement purification

Entanglement purification can probabilistically generate fewer highly entangled states from many weakly entangled ones. For example, in the extreme-photon-loss protocol, a highly entangled state is generated from two weakly entangled states. The following paragraph explains this protocol.

In order to distill the two quantum states that can be represented by Equation 3.6, in other words to remove the term of $|00\rangle$, the process depicted in Figure 3.1 is performed. CNOT gates are applied to communication qubits at both nodes using the memory qubit as the control qubits. The communication qubit is then measured at both nodes, which proceed to share their measurement results. If the result is 11, the resulting state is shown in Equation 3.7. It is not important whether or not each quantum state is stored in which type of qubit, but it is general that a final entangled state is stored in the memory qubit that is less susceptible to noise. If the time difference with which the two quantum states are obtained is small, we can obtain the proper quantum state after distillation even if we do not know the phase ϕ . When the measurement outcome is different from 11, the protocol fails and the final state is still a weakly entangled state.

$$|\Psi_{AB}\rangle = e^{i\phi} \left[\frac{1}{\sqrt{2}} (|01\rangle + |10\rangle) \right] \quad (3.7)$$

3.2.1 Extreme-photon-loss protocol

The Extreme-photon-loss protocol can generate high-quality entangled states by distilling two weakly-entangled states created by the single-click protocol. The entire process of creating a entangled state is described in Figure 3.2.

(step 1) Generating entanglement by single-click

As described in Section 3.2, mixed state, i.e., a weakly entangled state, in Equation 3.5 is generated.

(step 2) Swap between communication qubit and memory qubit

The communication qubit must be freed up so that the node can again attempt entanglement generation. Therefore, we swap the quantum state into memory qubit.

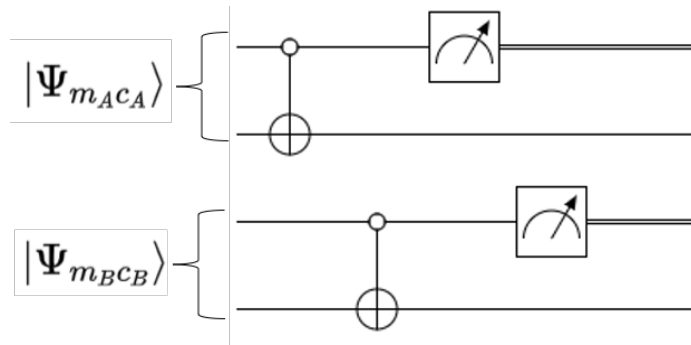


Figure 3.1: Quantum circuit of entanglement purification; CNOT gates are applied to communication qubits at both nodes using the memory qubit as the control qubits. The communication qubit is then measured at both nodes and the results are sent to the other node. If the result is 11, the entangled state can be obtained. $|\Psi_{m_A}\rangle$ represents the state in memory qubit at node A. $|\Psi_{c_A}\rangle$ represents the state in communication qubit at node A.

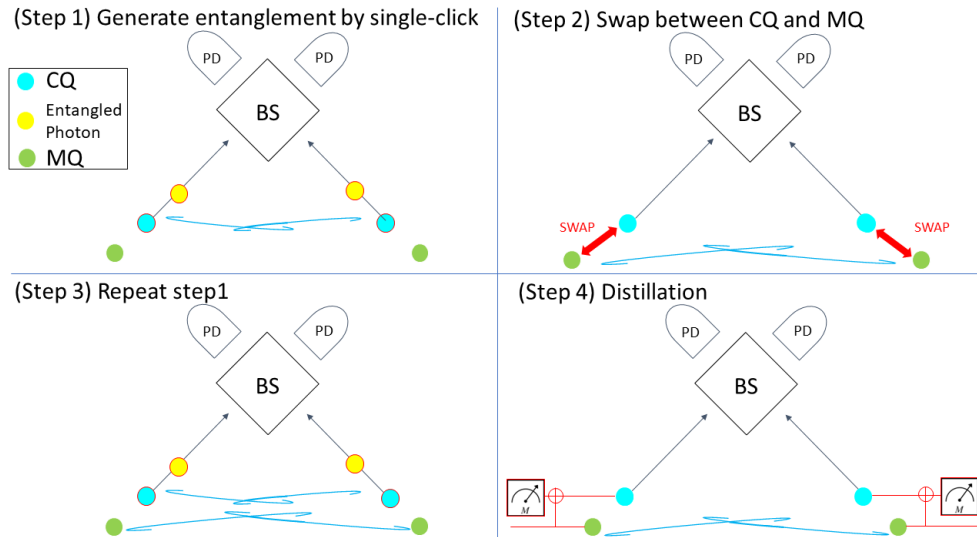


Figure 3.2: Extreme-photon-loss entanglement generation protocol; In step 1, the CQ states in both nodes are entangled through a single-click protocol. In step 2, the states stored in the CQs are swapped to the MQs; in step 3, the same as step 1 is done. In step 4, the CQ and MQ are distilled, and finally the entangled state is stored in the memory qubit. The PD stands for photon detector and BS stands for beam splitter.

(step 3) Repeat step 1

(step 4) Distillation

Perform the entanglement generation protocol described in [Section 3.2](#). If the measurement outcomes are 11, the protocol concludes successfully. Otherwise, go back to step 1.

3.2.2 Barrett-Kok protocol

The single-click protocol inherently has fidelity less than 1, even in the absence of noise. In double-click protocols, on the other hand, this trade-off is not present. These are protocols in which success is heralded by the detection of two photons. In the Barrett-Kok protocol proposed by Barrett et al. in 2005 [[Barrett and Kok, 2005](#)], the single-click protocol described in the [Section 3.2](#) is performed twice in succession, effectively requiring two photons to be measured. More generally, double-click protocols can be performed using any suitable degree of freedom, such as polarization or time-bin [[Simon and Irvine, 2003](#)]. Due to this fact, the entanglement generation probability is proportional to the square of the transmission efficiency in both cases. Therefore, if the transmission efficiency is smaller than 1, the success probability of quantum entanglement generation is generally lower than for single-click protocol.

(step 1)

In the Barrett-Kok protocol, the quantum states of both nodes are first set to the state of $|+\rangle = (|0\rangle + |1\rangle)/\sqrt{2}$. Then the bright state is excited using a laser. After traveling through the fiber, the photon arrives at a beam splitter and the state shown in [Equation 3.8](#) is obtained. m denotes the matter and p denotes the photon.

$$\begin{aligned} |\Psi_{m_A m_B p_A p_B}\rangle &= \frac{1}{2}|11\rangle|00\rangle \\ &+ \frac{1}{2}\left[\frac{1}{\sqrt{2}}(-i|01\rangle + |10\rangle)|01\rangle + \frac{1}{\sqrt{2}}(|01\rangle - i|10\rangle)|10\rangle\right] \\ &- \frac{i}{4}|00\rangle(|20\rangle + |02\rangle) \end{aligned} \quad (3.8)$$

(step 2)

After the beam splitter, two photon detectors are placed as shown in step 1 of [Figure 3.2](#). If only one of the detectors detects a photon, e.g., the photon of system p_A , then we will have the mixed state shown in [Equation 3.9](#) of $|01\rangle - i|10\rangle$ (If the photon of system p_B is detected, $-i|01\rangle + |10\rangle$) and $|00\rangle$.

$$\begin{aligned} |\Psi_{m_A m_B}\rangle &= \frac{2}{\sqrt{5}}\left[\frac{1}{\sqrt{2}}(|01\rangle - i|10\rangle) - \frac{i}{2}|00\rangle\right] \text{ or} \\ &= \frac{2}{\sqrt{5}}\left[\frac{1}{\sqrt{2}}(-i|01\rangle + |10\rangle) - \frac{i}{2}|00\rangle\right] \end{aligned} \quad (3.9)$$

(step 3-1)

The next step is to apply an X gate to the matter of both nodes. We change the quantum state of $|00\rangle$ into $|11\rangle$, a state in which no photons can be emitted, without changing the quantum state of $|01\rangle - i|10\rangle$ (or $-i|01\rangle + |10\rangle$) up to a phase. After waiting for any remaining excited states to relax, photon detection heralds the entangled state shown in [Equation 3.10](#). If the photon is detected by the same detector

as step 2, the final state will be $|\psi_+\rangle$, if detected by different detectors, it will be $|\psi_-\rangle$.

$$\rho_{m_A m_B} = |\psi_+\rangle\langle\psi_+| \text{ or } |\psi_-\rangle\langle\psi_-|, \text{ with } |\psi_\pm\rangle = (|01\rangle \pm |10\rangle) / \sqrt{2} \quad (3.10)$$

(step 3-2)

If photons are not detected after applying X gates and waiting for the further time for relaxation, we re-start from step 1 again.

3.3 TIME-MULTIPLEXED ENTANGLEMENT GENERATION

The single-click and double-click protocols described in [Section 3.2](#) tend to have low success probabilities. This is because the probability of collecting the photons into the fiber once they have been emitted is small and the probability of photon loss in a fiber is very large [[Tanzilli et al., 2005](#)]. One way to improve the success probability is to perform many entanglement generation attempts in parallel, which is called multiplexing. There are several types of multiplexing methods: time multiplexing, spectral multiplexing and spatial multiplexing [[Collins et al., 2007](#); [Munro et al., 2010](#); [Sinclair et al., 2014](#)].

Here, we will focus on the time multiplexing method, which can be achieved by the process shown in [Figure 3.3](#). This has two advantages: first, the average time for generating entanglement can be reduced by a factor of order N, with N being the number of used memory qubits, compared to the non-time multiplexing protocols. Second, states can be held in memory qubits, which tend to have a longer coherence time than communication qubits.

On the other hand, it has limitations. First, swapping the state from the communication to the memory qubit inevitably introduces noise, reducing the state's fidelity. However, it might be that this decrease in fidelity is still compensated by the fact that the state is then held in a memory qubit, which has a longer coherence time. In addition, the time a swap takes might be too long for some platforms. For example, if the distance between the heralding station and a node is 20 km, an entanglement generation attempt takes 0.2 ms. If the swap time is larger than this communication time then time-multiplexing is not useful.

Time multiplexing protocol

(step 1) Perform an entanglement generation attempt.

(step 2) Swap between the communication qubit and a memory qubit.

(step 3) After the swap, repeat step 1 and step 2 until success is heralded.

3.4 ENTANGLEMENT SWAP

Entanglement swaps, which are applications of quantum teleportation, allow for glueing together short entangled links to make longer ones. By using entanglement swap, we can connect two elementary links so that longer entangled links are finally generated between two distant nodes. Quantum teleportation is method for transferring a quantum state stored in one node to a distant node, and can be performed as shown in [Figure 3.4](#).

Incidentally, if a state of one quantum system that is entangled with another quantum system is determined, then the state of the second one is also instantaneously determined. Since this happens regardless of the distance between the two particles,

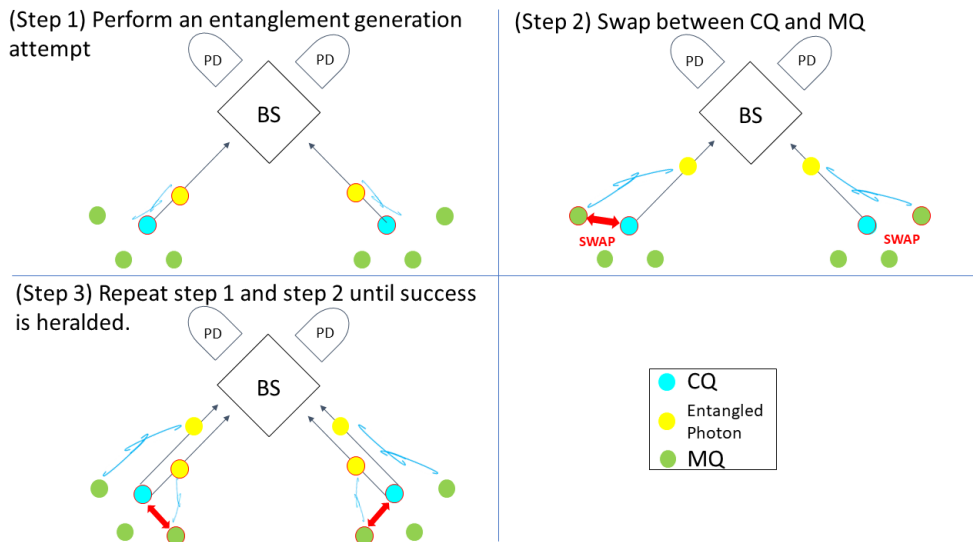


Figure 3.3: Time-multiplexed entanglement generation. The protocol starts with performing an entanglement generation attempt. (step 1). The CQ is swapped immediately to the MQ (step 2). After the swap, repeat step 1 and step 2 until success is heralded (step 3). The PD stands for photon detector and BS stands for beam splitter [Dam et al., 2017].

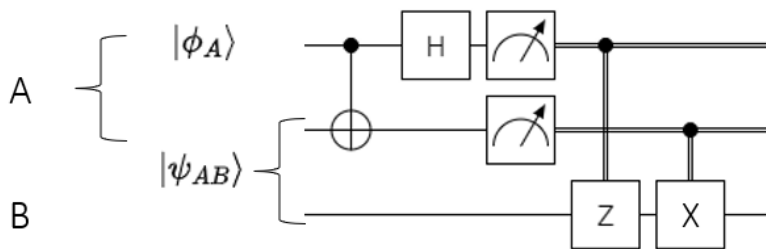


Figure 3.4: Quantum circuit for entanglement teleportation. By applying CNOT gate and Hadamard gate, make entanglement between $|\phi_A\rangle$ and the qubit of $|\psi_{AB}\rangle$ held by node A. Both states in node A are measured in the computational basis, which results in one four possible different outcomes. Node A sends the measurement results to node B. Then, node B applied Z or X gate on the state which node B has based on the results.

the entanglement is the basis for quantum teleportation [Bennett et al., 1993].

Quantum teleportation

As a setup for the quantum teleportation, two nodes A and B share the entangled state $|\psi_{AB}\rangle$ and the node A wants to send $|\phi_A\rangle$ to node B.

(step 1)

Apply a CNOT gate to the qubit of $|\psi_{AB}\rangle$ held by node A with $|\phi_A\rangle$ as the control qubit, followed by a H gate on $|\phi_A\rangle$.

(step 2)

Both states in node A are measured in the computational basis, which results in one four possible different outcomes: 00 or 01 or 10 or 11.

(step 3)

A sends the measurement results to B. Then, B applies Z or X gate on the state based on the results. When we assume that a is the node A's measurement outcome and b is the node B's one, the node B applies $Z^b X^a$ on his state.

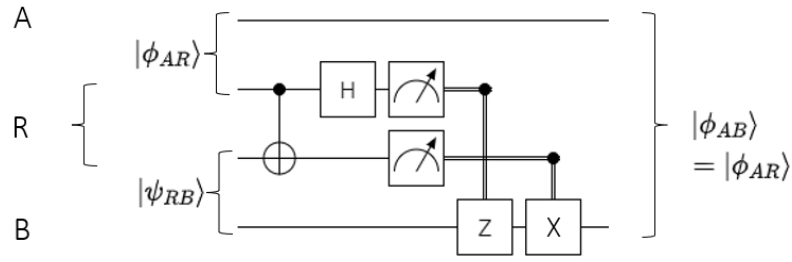


Figure 3.5: Quantum circuit for entanglement swap. Node A and node B each share an entangled state, $|\psi\rangle$ and $|\phi\rangle$, with the repeater node. In the repeater, the two photons are entangled. After that, the same process of entanglement teleportation is conducted.

Through quantum teleportation, we can transfer quantum information between distant nodes. In short, by using the entanglement swap protocol, an entangled state can be shared between distant nodes. In the entanglement swap protocol, two (entangled) states instead of the $|\phi_A\rangle$ prepared in step 1 of quantum teleportation are prepared and one of them is sent to the repeater. Then, by teleporting this qubit, the entangled state $|\phi\rangle$ is shared between A and B. The specific method is shown in [Figure 3.5](#).

Entanglement swap

As a setup for the entanglement swap, node A and node B each share an entangled state, $|\psi\rangle$ and $|\phi\rangle$, with a repeater node. The repeater is an intermediate node between A and B.

(step 1)

In the repeater, a CNOT gate is applied to the quantum state which is entangled with B, with a qubit in node A as control qubit. Then, an H gate is applied to it.

(step 2)

Both states in the repeater are measured in the computational basis, then obtaining four possible outcomes.

(step 3)

The repeater sends the measurement results to B. Then, a Z and/or X gate is applied to the qubit based on the results at node B. When we assume that a is the measurement outcome of the node R's state entangled with the state in node A and b is the measurement outcome of the node R's state entangled with the state in node B, the node B applies $Z^b X^a$ on his state.

Entanglement swap allows entangled states to be shared between two distant nodes.

3.5 QUANTUM REPEATER HARDWARE PLATFORM

There are several different physical systems being considered as possible platforms for realizing quantum repeaters such as Nitrogen-vacancy (NV) center in diamond, trapped-ions [[Zwinger et al., 2017](#)], and atomic ensembles [[Sangouard et al., 2009](#)]. Each platform has its advantages and disadvantages, and it is important to consider the trade-offs between them. The advantages and disadvantages of each platform are described in this section. In our research, we do not focus on a particular implementation and focus on processing-node repeaters. So, the atomic ensembles

platform is not captured by our work.

NV Center

NV centers consist of a diamond lattice in which one of the carbon atoms has been replaced by a nitrogen atom, next to a vacancy in the lattice. This gives rise to an optically-active electronic spin that can be used as a communication qubit. Around the vacancy, there are naturally 1% isotope of carbon ^{13}C which can couple to nearby electron spins. It can act as a memory qubit which has long coherence time. C. E. Bradley et al. achieved coherence times of a few seconds for individual nuclear spin qubits under dynamical decoupling [Bradley et al., 2019]. An NV center can then be seen as a quantum processor with a star topology [Zhu and Ma, 2018], with the communication qubit in the center and the memory qubits surrounding it. This means that the communication qubit can interact with the memory qubits, but these cannot interact directly with one another.

NV centers are good candidates for realizing quantum repeaters, having already demonstrated many required primitives such as purification, entanglement generation and teleportation. Kalb et al. achieved purification of distant electron-nuclear two-qubit nodes using combination of generating, holding in memory and processing distant entangled qubits [Kalb et al., 2017]. Humphreys et al. demonstrated 39 Hz of entanglement generation between nodes 2 meters apart [Humphreys et al., 2018]. Hermans et al. demonstrated quantum teleportation between remote, non-neighboring nodes using three-node network with approximately 70% fidelity in about 10 ms [Hermans et al., 2021]. Swap gate was also demonstrated in relatively short time by J. Cramer et al. [Cramer et al., 2016].

Note that NV centers have only one communication qubit, therefore a swap between communication qubit and memory qubit must be completed in time-multiplexing protocol before a new photon can be emitted.

Trapped-ion

An ion trap consists of multiple ions confined by electromagnetic fields. These ions are trapped in ultrahigh vacuum and are isolated from the outside world. They are also cooled down to a temperature of approximately a few μK by laser cooling, so they remain still. Incidentally, the trapped-ion system is not only used for quantum repeaters, but is also one of the leading platforms to realize quantum computers. C. Monroe founded IonQ in 2015 and has been focusing on research to realize a large scale quantum computer using the trapped ion system [D.Kielinski and Monroe, 2002].

Malinovsky et al. [Malinovsky et al., 2019] presented a repeater architecture based on dual-species trapped-ion (DSTI) modules with lasers and light collection apparatuses. This combination of different ions can achieve required property for the quantum repeaters. For example, $^{138}\text{Ba}^+$ ion can emit a photon so that it can perform as communication qubits. By using several $^{138}\text{Ba}^+$ ion in a module, we can say that multiple communication qubit can be incorporated into a node. $^{171}\text{Yb}^+$ ions, which has better coherence time, serve as the memory ions. Actually, for a single qubit quantum memory of $^{171}\text{Yb}^+$, 10 minute of coherence time have been reported by Wang et al. [Wang et al., 2017]. By the lasers, operations on these ions are performed, but since the transition frequencies of the two ions are different, they can be controlled without interference. Malinovsky et al. proposed swap gate model between a memory qubit and a communication qubit. Besides, they also proposed entanglement swap between memory ions using CNOT gate, X or Z measurement and heralded entanglement generation between communication ions at different nodes.

The group of Ben Lanyon at the University of Innsbruck uses Ca^+ ion for communication qubit because it has low noise when it is converted from a trapped-ion

wavelength (854 nm) to telecom (1550 nm), which is useful frequency for a fiber communication. Note that there is no distinction between memory qubit and communication qubit. Therefore, the coherence time for the communication qubit and the memory qubit in the trapped-ion is reported as 85 ms by them. In this research, we use this value for the coherence time of the communication qubit and the memory qubit [[Krutyanskiy et al., 2022](#)].

4

EFFECT OF HARDWARE IMPERFECTIONS ON SKR

In [Chapter 4](#), we will investigate the impact of different hardware parameters on the SKR that can be achieved by two nodes connected without a repeater (i.e., in an elementary link).

4.1 MODELS

In this section, we will explain problem setups for the following three research questions:

- For which parameter regimes does time-multiplexing allow for getting higher SKR than without multiplexing?
- Which hardware parameters are most important for improving SKR?
- What is the impact of the number of CQs on the SKR?

4.1.1 Common settings

For all experiments in [Chapter 4](#), we assume that there are two end nodes 100 km apart and that a heralding station with two photon detectors and a beam splitter lies in the middle. In this setup, the hardware parameter values shown in [Table 4.1](#) are assumed. On the other hand, values of depolarizing noise at swap gate, swap gate time and number of CQ (MQ), and number of memory qubits used in a node (N_{max}) are different for each research question and will be explained again in each subsection.

Hardware modeling

Here, we introduce our modeling for the setup we consider in [Chapter 4](#).

Overall system transmission efficiency (η)

The probability that a photon is emitted from each node and reaches the heralding station can be calculated by multiplying the following three parameters: coupling efficiency, frequency conversion efficiency, and fiber loss. Photons excited at the NV center or trapped-ion platform need to be collected on a communication fiber. We assume that with probability p_{out} the coupling succeeds, and with probability $1 - p_{out}$ the photon is lost. The wavelength band that is favorable for transmitting photons over long distances is different from the wavelength band that allows photons to interact with matter [[Krutyanskiy et al., 2017](#)]. Therefore, it is necessary to perform frequency conversion. The frequency conversion efficiency is p_{fc} . Finally, as we mentioned in [Section 3.1](#), loss in fiber can be represented as $10^{-d p_{loss}/20}$, since photon loss grows exponentially with distance. Therefore, the overall system transmission efficiency can be calculated by $\eta = p_{out} p_{fc} 10^{-d p_{loss}/20}$.

Number of memory qubits used in a node (N_{max})

We assume that N_{max} , which is the maximum number of MQs that a node can use assuming a number of CQ and an entanglement generation protocol, is deployed in each node in all experiments. For example, in the mSC protocol, the value can be calculated by $N_{max} = \lceil \frac{T_{att}}{T_{sg}} \rceil$. The numerator (T_{att}) represents the time it takes for a photon to reach the heralding station and for the result to return to the original node. The denominator (T_{sg}) represents the time it takes to perform a swap between the communication qubit and the memory qubit. N_{max} can be calculated by applying the ceiling function to this fraction. To be accurate, the coefficients multiplied by the formula or variables in the formula, $N_{max} = \lceil \frac{T_{att}}{T_{sg}} \rceil$, depend on the entanglement generation protocol and the number of CQs. Therefore, the exact values will be mentioned when the model is introduced for each experiment.

Memory decoherence (T_m)

We assume a depolarizing noise model, which is worst-case scenario, for both the memory qubits and the communication qubits. Then, we can model the depolarizing noise using $p_m = 1 - e^{-\frac{t}{T_m}}$ as shown in Equation 4.1. T_m is coherence time that it takes for a state to lose $1/e$ of its information and gain a random state in memory (communication) qubit. t represents elapsed time. In the same way, we apply this model to CQ using coherence time of CQ (T_c).

$$\rho_{dep} = (1 - p_m)\rho + \frac{p_m}{4}I_4 \quad (4.1)$$

Depolarizing noise at swap gate (p_{depsg})

We assume that depolarizing noise is introduced when performing swap gate with probability p_{depsg} .

Hardware parameter values

The values of some of the parameters used in the experiments for Chapter 4 are shown in Table 4.1.

Overall system transmission efficiency (η)

We assume the coupling efficiency (p_{out}) of 0.3 as in [Dam et al., 2017]. Besides, we assume that the frequency conversion efficiency (p_{fc}) is 0.3 as in [Zaske et al., 2012]. We also assume p_{loss} to be 0.2 dB/km for the same reason. Therefore, the overall system transmission efficiency can be calculated by $\eta = p_{out}p_{fc}10^{-0.2d/20} = 0.3 \times 0.3 \times 10^{-0.2 \times 100/20} = 0.009$.

Number of memory qubits used in a node (N_{max})

The coefficients multiplied by the formula or variables in the formula, $N_{max} = \lceil \frac{T_{att}}{T_{sg}} \rceil$, depend on the entanglement generation protocol and the number of CQs. Therefore, the exact values will be mentioned when the model is introduced for each experiment.

Table 4.1: Common parameter settings. The parameters used in all the experiments of [Chapter 4](#) are listed. Basically, they are based on experimentally realized values. η is the probability that a photon is emitted from each node and reaches the heralding station. p_{fc} is the frequency conversion efficiency from the NV center or the trapped ion wavelength to a telecom fiber. p_{loss} is the probability that a coupling succeeds from the matter to the fiber. N_{max} is the maximum number of MQs that a node can use assuming a number of CQ and an entanglement generation protocol. $T_m(T_c)$ is the coherence time of MQ (CQ). T_{sg} is the swap gate time. p_{depsg} is the probability of introducing depolarizing noise when performing the swap gate. α' is the probability of generating entangled states in [Equation 3.5](#). d is the distance between two end nodes. c is the photon speed in a fiber.

Parameters	NV center	Trapped-ion
η	0.009 [Dam et al., 2017 ; Zaske et al., 2012]	
p_{fc}	0.3 [Zaske et al., 2012]	
$p_{loss}[\text{dB}/\text{km}]$	0.2	
N_{max}	depends on entanglement generation protocol	
$T_m[\text{s}]$	1 [Bradley et al., 2019]	0.085 [Krutyanskiy et al., 2022]
$T_c[\text{s}]$	0.5 [Pompili et al., 2021]	0.085 [Krutyanskiy et al., 2022]
$T_{sg}[\mu\text{s}]$	200 [Cramer et al., 2016]	3000 [Schupp et al., 2021]
p_{depsg}	0.17 [Hermans et al., 2021]	0.06 [Krutyanskiy et al., 2022]
α' (in Equation 3.5)	0.1	
$d[\text{km}]$	100	
$c[\text{km}/\text{s}]$	200000	

Memory decoherence

We assume the coherence time of MQ of 1 s [[Bradley et al., 2019](#)] and the coherence time of CQ of 0.5 s [[Pompili et al., 2021](#)] for NV center. For trapped ions, we assume 85 ms for both values [[Krutyanskiy et al., 2022](#)], as reported by the group of Ben Lanyon at the University of Innsbruck.

Swap gate time (T_{sg})

In [Chapter 4](#), several simulations assuming that this parameter has been improved have also been investigated. Therefore, we show the experimentally realized value below, but note that we do not necessarily use this value. For NV centers, we assume $T_{sg} = 200\mu\text{s}$, which may be feasible in the near-term [[Cramer et al., 2016](#)]. For trapped ions, we assume an experimentally realized value of 3 ms [[Schupp et al., 2021](#)].

Depolarizing noise at swap gate (p_{depsg})

In [Chapter 4](#), several simulations assuming that this parameter has been improved have also been investigated. Therefore, we show the experimentally realized value below, but note that we do not necessarily use this value. For the NV center, 0.17 is assumed as experimentally realized value [[Hermans et al., 2021](#)]. For the trapped ion, 0.06 is assumed as experimentally realized value [[Krutyanskiy et al., 2022](#)].

The other parameters

α' is the probability of generating entangled states in [Equation 3.5](#) and we assume that α' is 0.1. We assume that the distance between the two end nodes (d) is 100 km and the photon speed in a fiber (c) is 200,000 km/s. Therefore, combined quantum

and classical communication time required to know whether a photon click or not at the heralding station, T_{att} , is 0.5ms. Incidentally, we assume that gates and measurements in the distillation protocol are done perfectly.

Rate and quality of entangled states

We use the following four protocols in our thesis: single-click (SC), time-multiplexed SC (mSC), time-multiplexed extreme-photon loss (mEPL), and time-multiplexed Barrett-Kok (mBK). Therefore, we show the calculation process of the entanglement generation rate and SKF for the four protocols. We assume that the target entangled state is $|\psi_+\rangle$ in all protocols.

Calculation of secret key fraction

SC

Here, we show how the final state shared by the two nodes is derived. We start by generating entanglement between node A and node B by single-click protocol and get the state as shown in Equation 4.2 which is the same as Equation 3.5. $\rho_{c_a c_b}$ represents the state in a CQ at the node A(B)

$$\rho_{c_a c_b} = (1 - \alpha')|\Psi_+\rangle\langle\Psi_+| + \alpha'|00\rangle\langle 00| \quad (4.2)$$

Furthermore, the state decoheres in the CQ. When we set $t = 0$ as the time immediately after the entangled state is generated, the state at time t can be represented by Equation 4.3. $p_c = 1 - e^{-\frac{t}{T_c}}$, which represents how much the state in CQ has decohered.

$$\rho_{c_a c_b} = (1 - p_c) [(1 - \alpha')|\Psi_+\rangle\langle\Psi_+| + \alpha'|00\rangle\langle 00|] + \frac{p_c}{4} I_4 \quad (4.3)$$

Using this state, the quantum bit error rate (QBER ($Q_x(Q_z)$)) can be calculated by Equation 4.4.

$$\begin{aligned} Q_x &= Pr((x_A = 0 \wedge x_B = 0) \vee (x_A = 1 \wedge x_B = 1)) \\ &= \langle 00 | \rho_{c_a c_b} | 00 \rangle + \langle 11 | \rho_{c_a c_b} | 11 \rangle \\ Q_z &= Pr((x_A = 0 \wedge x_B = 0) \vee (x_A = 1 \wedge x_B = 1)) \\ &= \langle ++ | \rho_{c_a c_b} | ++ \rangle + \langle -- | \rho_{c_a c_b} | -- \rangle \end{aligned} \quad (4.4)$$

The SKF can be calculated by substituting these quantum bit error rates into Equation 2.25.

mSC

Here, we show how the final state shared by the two nodes is derived. We start by generating entanglement between node A and node B by the single-click protocol. Then, the state is swapped from the CQ to an MQ, resulting in the state shown in Equation 4.5. $\rho_{m_a m_b}$ represents the state in an MQ at node A (B).

$$\rho_{m_a m_b} = \left(1 - p_{\text{depsg}}\right) [(1 - \alpha')|\Psi_+\rangle\langle\Psi_+| + \alpha'|00\rangle\langle 00|] + \frac{p_{\text{depsg}}}{4} I_4 \quad (4.5)$$

Furthermore, the state decoheres in the MQ. When we set $t = 0$ as the time immediately after the entangled state is generated, the state at time t can be represented

by Equation 4.6. $p_m = 1 - e^{-\frac{t}{T_m}}$ represents how much the state in MQ has decohered.

$$\begin{aligned} \rho_{m_a m_b}(t) &= (1 - p_m) \left\{ (1 - p_{\text{depsg}}) [(1 - \alpha') |\Psi_+\rangle \langle \Psi_+| + \alpha' |00\rangle \langle 00|] + \frac{p_{\text{depsg}}}{4} I_4 \right\} \\ &+ \frac{p_m}{4} I_4 \end{aligned} \quad (4.6)$$

Using this state, the QBER ($Q_x(Q_z)$) can be calculated by Equation 4.7.

$$\begin{aligned} Q_x &= Pr((x_A = 0 \wedge x_B = 0) \vee (x_A = 1 \wedge x_B = 1)) \\ &= \langle 00 | \rho_{m_a m_b} | 00 \rangle + \langle 11 | \rho_{m_a m_b} | 11 \rangle \\ Q_z &= Pr((x_A = 0 \wedge x_B = 0) \vee (x_A = 1 \wedge x_B = 1)) \\ &= \langle ++ | \rho_{m_a m_b} | ++ \rangle + \langle -- | \rho_{m_a m_b} | -- \rangle \end{aligned} \quad (4.7)$$

The SKF can be calculated by substituting these quantum bit error rates into Equation 2.25.

mEPL

Here, we show how the final state shared by the two nodes is derived. We start by generating entanglement between node A and node B by time-multiplexed single-click protocol and get the same state as Equation 4.6.

$$\begin{aligned} \rho_{m'_a m'_b}(t) &= (1 - p_m) \left\{ (1 - p_{\text{depsg}}) [(1 - \alpha') |\Psi_+\rangle \langle \Psi_+| + \alpha' |00\rangle \langle 00|] + \frac{p_{\text{depsg}}}{4} I_4 \right\} \\ &+ \frac{p_m}{4} I_4 \end{aligned} \quad (4.8)$$

Then, we create the second entangled state by the same process, and get the state as shown in Equation 4.6.

Then we will do distillation using these two states, $\rho_{m'_a m'_b}(t = T_{att} - T_{sg})$ and $\rho_{m_a m_b}(t = \frac{1}{x''} + T_{att} - T_{sg})$, immediately after the second entangled state ($\rho_{m_a m_b}(t)$) is generated. We consume $\rho_{m_a m_b}$ by the distillation. x'' represents the rate of entanglement generation to generate the second entangled state. Since an entangled state is already stored in one memory, $x'' = (N_{max} - 1)\eta\alpha'/T_{att}$. Incidentally, in the same way, the first entanglement generation rate (x') is $N_{max}\eta\alpha'/T_{att}$. All states after applying the two CNOT gates in the distillation step can be calculated by Equation 4.9. U_1 is CNOT operator using m_a as the target qubit and m'_a as the control qubit. U_2 is CNOT operator using m_b as the target qubit and m'_b as the control qubit.

$$\rho_{m_a m_b m'_a m'_b} = U_2 U_1 (\rho_{m_a m_b}(t' = \frac{1}{x''} + T_{att} - T_{sg}) \otimes \rho_{m'_a m'_b}(t = T_{att} - T_{sg})) U_1^+ U_2^+ \quad (4.9)$$

Then, $\rho_{m_a m_b}$ is measured, and the final state of $\rho_{m'_a m'_b}$ can be calculated by Equation 4.10. $P_{11} = |1\rangle\langle 1| \otimes |1\rangle\langle 1| \otimes I_2 \otimes I_2$ is the projective operator when both measurement results are 1. Also, $P_i = \text{Tr}[P_{11} \rho_{m_a m_b m'_a m'_b}]$ is the probability that both measurement results are 1.

$$\rho_{m'_a m'_b} = \text{Tr}_{m_a m_b} \left[\frac{P_{11} \rho_{m_a m_b m'_a m'_b} P_{11}}{P_i} \right] \quad (4.10)$$

Using this state, the QBER ($Q_x(Q_z)$) can be calculated by [Equation 4.11](#).

$$\begin{aligned} Q_x &= Pr((x_A = 0 \wedge x_B = 0) \vee (x_A = 1 \wedge x_B = 1)) \\ &= \langle 00 | \rho_{m'_a m'_b} | 00 \rangle + \langle 11 | \rho_{m'_a m'_b} | 11 \rangle \\ Q_z &= Pr((x_A = 0 \wedge x_B = 0) \vee (x_A = 1 \wedge x_B = 1)) \\ &= \langle ++ | \rho_{m'_a m'_b} | ++ \rangle + \langle -- | \rho_{m'_a m'_b} | -- \rangle \end{aligned} \quad (4.11)$$

The SKF can be calculated by substituting these quantum bit error rates into [Equation 2.25](#).

mBK

Here, we show how the final state shared by the two nodes is derived. We start by generating entanglement between node A and node B by the Barrett-Kok protocol and get the same state as [Equation 3.10](#). We assume the process succeeds deterministically and will compensate for the assumption by considering the actual success probability when calculating the entanglement generation rate. After the first photon is emitted, we swap the state from CQ to MQ and get the state as shown in [Equation 4.12](#). In our experiment, it is assumed that only $|\psi_+\rangle$ is generated, since we can anyway perform correction.

$$\rho_{m_a m_b} = (1 - p_{depsg}) |\Psi_+\rangle \langle \Psi_+| + \frac{p_{depsg}}{4} I_4 \quad (4.12)$$

When we assume $t=0$ is the time immediately after the end of swap, the final state is generated at $t = 2T_{att} - T_{sg}$ as shown in [Equation 4.13](#).

$$\rho_{m_a m_b}(t) = (1 - p_m) \left\{ (1 - p_{depsg}) |\Psi_+\rangle \langle \Psi_+| + \frac{p_{depsg}}{4} I_4 \right\} + \frac{p_m}{4} I_4 \quad (4.13)$$

Using this state, the QBER ($Q_x(Q_z)$) can be calculated by [Equation 4.14](#).

$$\begin{aligned} Q_x &= Pr((x_A = 0 \wedge x_B = 0) \vee (x_A = 1 \wedge x_B = 1)) \\ &= \langle 00 | \rho_{m_a m_b} | 00 \rangle + \langle 11 | \rho_{m_a m_b} | 11 \rangle \\ Q_z &= Pr((x_A = 0 \wedge x_B = 0) \vee (x_A = 1 \wedge x_B = 1)) \\ &= \langle ++ | \rho_{m_a m_b} | ++ \rangle + \langle -- | \rho_{m_a m_b} | -- \rangle \end{aligned} \quad (4.14)$$

The SKF can be calculated by substituting these quantum bit error rates into [Equation 2.25](#).

Calculation of entanglement generation rate

SC

- The entanglement generation rate can be calculated by $\eta \alpha' / T_{att} = 1.8(\text{Hz})$.
- $\eta = 0.3 \times 0.3 \times 10^{-0.2 \times 100 / 20}$ is the overall system transmission efficiency.
- $\alpha' = 0.1$ is the probability of generating entangled states by the SC protocol and $T_{att} = d/c$ is 0.5ms.

mSC

- The entanglement generation rate can be calculated by $N_{max} \eta \alpha' / T_{att}$.
- When the number of CQ is 1, $N_{max} = \lceil \frac{T_{att}}{T_{sg}} \rceil$.

mEPL

- The entanglement generation rate can be calculated by $\frac{P_i}{\frac{1}{x'} + \frac{1}{x''}}$.
- When the number of CQ is 1, $N_{max} = \lceil \frac{T_{att}}{T_{sg}} \rceil$. When the number of CQ is 2, $N_{max} = 2 \lceil \frac{T_{att}}{T_{sg}} \rceil$.

mBK

- The entanglement generation rate can be calculated by $N_{max}\eta^2 \times 0.6/2T_{att}$.
- When the number of CQ is 1, $N_{max} = \lceil \frac{2T_{att}}{T_{sg}} \rceil$. When the number of CQ is 2, $N_{max} = 2 \lceil \frac{2T_{att}}{T_{sg}} \rceil$.
- The $0.6\eta^2$ in the numerator indicates the probability that the mBK protocol succeeds, calculated by multiplying the probability that the first click succeeds, $(3\eta/4)$, by the probability that the second click succeeds, $(4\eta/5)$.

4.1.2 For which parameter regimes does time-multiplexing allow for getting higher SKR than without multiplexing?

Experimentally realized values of the current parameters such as p_{depsg} , which are relevant with time-multiplexing protocol, are large. It results in the prediction that using time-multiplexing protocol using such values might not be currently useful [Dam et al., 2017]. Therefore, we would like to know how much improvement of a hardware parameter would allow a time-multiplexed protocol to achieve a better SKR than a non time-multiplexed protocol. To investigate it, we compare the SKRs of SC and mSC when we improve p_{depsg} from 0.17 (experimentally realized value in NV) to 0 (ideal value). For the other parameters, the experimentally realized values are used as described above. As a result, we try to see where the break-even point to get better SKR by mSC is for the parameter of p_{depsg} . Under this experiment, we fix the value of T_{sg} (200 μ s). Therefore, N_{max} in mSC is also fixed and calculated as three.

4.1.3 Which hardware parameters are most important for improving SKR?

Besides p_{depsg} , which improves fidelity, T_{sg} , which can improve both entanglement generation rate and fidelity, also contributes to improvement of SKR. Because of this, we would like to know which one can improve SKR more efficiently. To investigate it, we compare the improvement rate of SKR in the following two cases. The first case is that only the probability of depolarizing noise is improved from 0.17 (experimentally realized value in NV) to 1.7×10^{-4} (corresponding to 99.9 % improvement). The second case is the one where only the swap gate time is improved from 2×10^{-4} (experimentally realized value in NV) to 2×10^{-7} (corresponding to 99.9 % improvement). In the first case, N_{max} is fixed at 3. On the other hand, in the second case, the value will change from 3 to 2500, since the value depends on T_{sg} . In addition to mEPL, we also do the same experiment above using mBK.

4.1.4 What is the impact of the number of CQs on the SKR?

If the trapped ion is used as the platform, the number of communication qubits that limit N_{max} can be increased. In other words, a large number of memory qubits

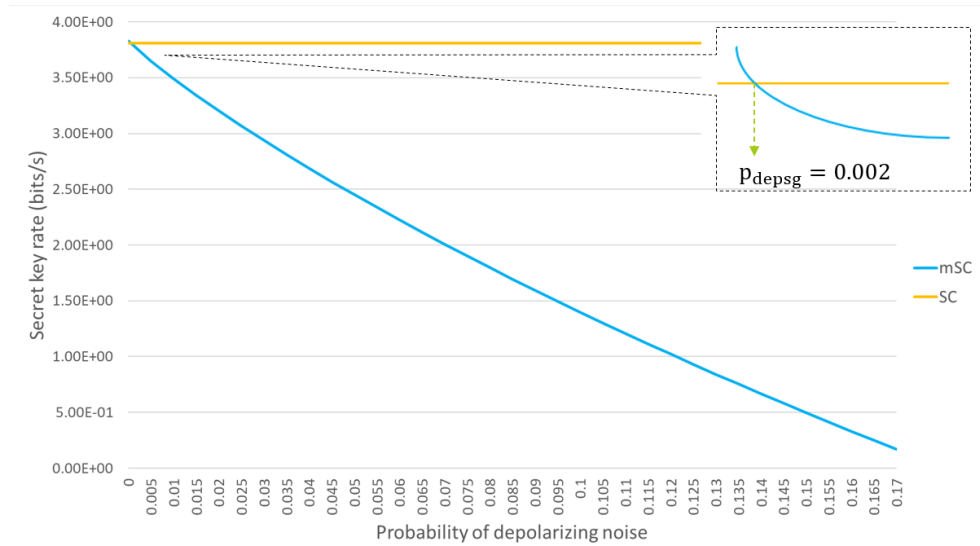


Figure 4.1: SKR when p_{depsg} is changed from the realistic value (0.17) to an ideal value (0). The yellow line represents the SKR of the SC protocol, and the blue line represents the SKR of the mSC protocol. We can see that mSC protocol yields higher SKR when p_{depsg} is less than 0.002.

can be implemented. As a result, the entanglement generation rate and SKF are increased, contributing to the improvement of SKR. Therefore, when changing the number of CQ from 1 to 2, we would like to know how much SKR can be improved in mEPL and mBK. We note that the same could be achieved with NV centers by placing multiple diamonds in one node. But in this research, we investigate only the trapped ion platform.

In the investigation of this research question, we use experimentally realized values in trapped-ions for every parameter except for the number of CQs. However, when we use the value for the parameter of T_{sg} , 3×10^{-3} , SKF is zero. Therefore, as for T_{sg} , we use three values, 3×10^{-5} (corresponding to 99 % improvement) or 3×10^{-6} (corresponding to 99.9 % improvement) or 3×10^{-7} (corresponding to 99.99 % improvement), for the parameter.

4.2 RESULTS

4.2.1 For which parameter regimes does time-multiplexing allow for getting higher SKR than without multiplexing?

From [Figure 4.1](#), we can see that it is not useful to perform time-multiplexing when using a single-click protocol unless p_{depsg} is improved to at most 0.002. As described before, the experimentally realized value of p_{depsg} in the NV centers is approximately 0.17, so there is no point in using mSC protocol unless it will be improved by 98.8 %. In this setup, N_{max} is three, and it turns out that this small amount of parallelism cannot compensate for the current large p_{depsg} , which has a significant negative impact on SKR. However, the dramatic improvement of p_{depsg} would be difficult to achieve in the near future. Therefore, improvement of the other parameters such as T_{sg} should be achieved simultaneously.

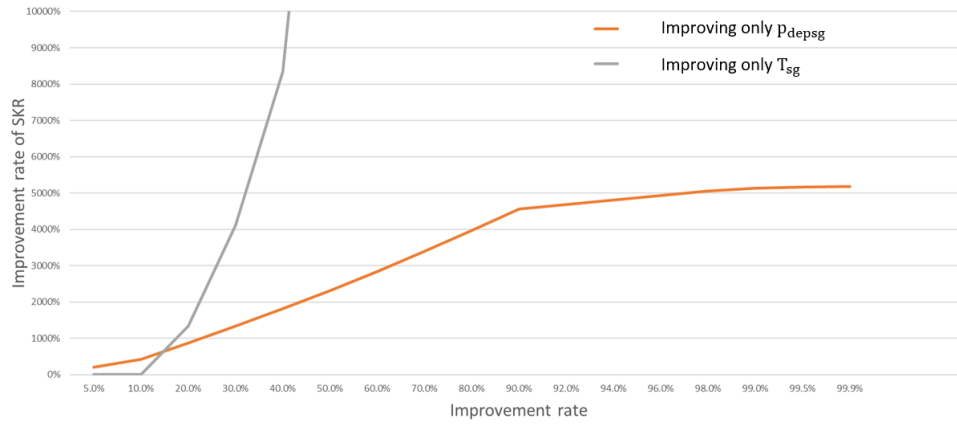


Figure 4.2: The improvement rate of SKR, (SKR using the improved values - SKR using the experimentally realized value) / SKR using the improved values, in the mEPL protocol are represented for the two cases. The orange line represents the first case where only the probability of depolarizing noise is improved from 0.17 (experimentally realized value) to 1.7×10^{-4} (99.9 % improved case compared to the value). The grey line represents the second case where only the swap gate time is improved from 2×10^{-4} (experimentally realized value) to 2×10^{-7} (99.9 % improved case compared to the value). With the case without any improvements for T_{sg} and p_{depsg} , the SKR is 0.007. For example, the improvement rate of p_{depsg} or T_{sg} is 15 %, the SKR is approximately 0.05 and the improvement rate of SKR is approximately 500 %.

4.2.2 Which hardware parameters are most important for improving SKR?

From [Figure 4.2](#), improving only T_{sg} has a larger impact on the improvement of SKR compared to the case of improving only p_{depsg} when they improve by more than approximately 15 % in mEPL protocols. When they improve by 15 %, the value of SKR is small (0.05). Therefore, it cannot be said that SKR is sufficiently improved considering use for real applications such as QKD. In addition, from [Figure 4.3](#), the same results can be seen when they are improved by more than approximately 77 % in the mBK protocols. When it is improved by 77 %, the value of SKR is also small (0.17). Therefore, it cannot be said that the SKR is improved enough. Hence, for both protocols, the improvement of T_{sg} is more important to obtain a better SKR.

As for mEPL, since the experimentally realized value of p_{depsg} is currently 0.17, the improvement rate of SKR is improved until 90 % improvement (0.017) is achieved. However, if the improvement rate is greater than 90 %, the impact on the improvement rate of SKR will be small because the SKR is already high. On the other hand, when only T_{sg} is improved, the improvement rate of SKR is also improved exponentially.

T_{sg} and N_{max} are in an inverse proportion. Therefore, the more T_{sg} is improved, the more N_{max} increases. This improves the entanglement generation rate exponentially. The SKR is also improved because the time until the second entangled state is generated is shortened. Thus, the improvement rate of SKR is improved exponentially. As for mBK, although we can reach the same result, its break-even point is slightly larger (approximately 77%) than mEPL.

On the other hand, it might be more difficult to improve T_{sg} than improving p_{depsg} . Therefore, we also have to consider trade-off between impact and feasibility.

4.2.3 What is the impact of the number of CQs on the SKR?

mEPL

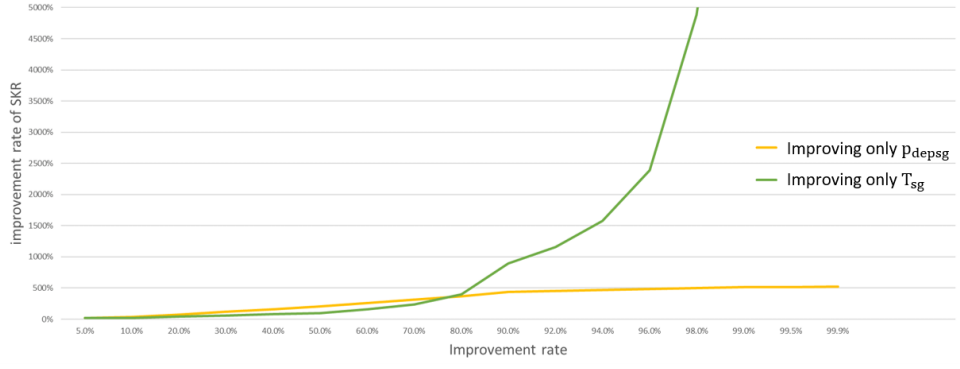


Figure 4.3: The improvement rate of SKR, (SKR using the improved values - SKR using the experimentally realized value) / SKR using the improved values, in the mBK protocol are represented for the two cases. The yellow line represents the first case where only the probability of depolarizing noise is improved from 0.17 (experimentally realized value) to 1.7×10^{-4} (99.9 % improved case compared to the value). The green line represents the second case where only the swap gate time is improved from 2×10^{-4} (experimentally realized value) to 2×10^{-7} (99.9 % improved case compared to the value). With the case without any improvements for T_{sg} and p_{depsg} , the SKR is 0.039. For example, the improvement rate of p_{depsg} or T_{sg} is 77 %, the SKR is approximately 0.17 and the improvement rate of SKR is approximately 350 %.

From the result of SKR using mEPL (Table 4.2), when $p_{depsg}=0.06$ and $T_{sg} = 3 \times 10^{-5}$, the SKR of mEPL (CQ=2) is improved by 452% compared to mEPL SKR (CQ = 1). When $p_{depsg}=0.06$ and $T_{sg} = 3 \times 10^{-6}$, SKR of mEPL (CQ=2) is improved by 113% compared to the SKR of mEPL (CQ=1). When $p_{depsg}=0.06$ and $T_{sg} = 3 \times 10^{-7}$, SKR of mEPL (CQ=2) is improved by 101% compared to the SKR of mEPL (CQ=1). From these results, we can see that the SKR and the entanglement generation rate increase proportionally to the number of CQs under ideal conditions of T_{sg} . SKF reaches the same value in the case of mEPL (CQ=1), if T_{sg} is ideally small.

The entanglement generation rate increases proportionally to the number of CQ. This is because N_{max} is proportional to the number of CQ and $\frac{P_i}{\frac{1}{x'} + \frac{1}{x''}}$ is also proportional to the number of CQ.

On the other hand, The two states before distillation, $\rho_{m'_a m'_b}(t = T_{att} - T_{sg})$ and $\rho_{m_a m_b}(t' = \frac{1}{x''} + T_{att} - T_{sg})$, converge to $\rho_{m_a m_b}(t' = T_{att})$ which has no relationship with T_{sg} under ideal T_{sg} . If T_{sg} is very small, N_{max} becomes large. Therefore, $1/x'' \ll T_{att}$ holds. As a result, SKF(CQ=1) and SKF(CQ=2) are almost the same.

Table 4.2: Entanglement generation rate, SKF and SKR in mEPL when changing the number of CQ. We can see that the SKR and the entanglement generation rate increase proportionally to the number of CQs under ideal conditions of T_{sg} . SKF reaches the same value in the case of mEPL (CQ=1), if T_{sg} is ideally small.

	$T_{sg}[s]$	Entanglement generation rate	SKF	SKR
mEPL(CQ=1)	3×10^{-5}	5.04	0.147	0.740
mEPL(CQ=2)	3×10^{-5}	10.9	0.375	4.08
mEPL(CQ=1)	3×10^{-6}	57.0	0.606	34.5
mEPL(CQ=2)	3×10^{-6}	115	0.641	73.6
mEPL(CQ=1)	3×10^{-7}	577	0.669	386
mEPL(CQ=2)	3×10^{-7}	116E+01	0.673	777

mBK

Under all parameter settings, the SKR of mBK (CQ=2) is improved by 100% compared to the SKR of mEPL (CQ=1) as shown in Table 4.3. The entanglement generation rate increases proportionally to the number of CQs. SKF is the same value in the case of mEPL (CQ=1) in every case.

As for entanglement generation rate, $\frac{P_i}{\frac{1}{x'} + \frac{1}{x''}}$, it is proportional to the number of CQ. On the other hand, SKF does not change, because the final state, $\rho_{m_a m_b}(t = 2T_{att} - T_{sg})$, is regardless of the number of CQs.

As a result, we can see that if T_{sg} is ideally small for both mEPL and mBK, the SKR increases proportionally to the number of CQ. However, the ideal T_{sg} is 1/10000 of the value of 3 ms which is an experimentally realized value in the trapped-ion and difficult to achieve. In cases where the improvement rate of T_{sg} is not high in mEPL, not only the entanglement generation rate but also SKF are improved, so that the number of CQs has more than twice the impact on SKR.

Table 4.3: Entanglement generation rate, SKF and SKR in mBK when changing the number of CQ. Under all parameter settings, the SKR of mBK (CQ=2) is improved by 100% compared to the SKR of mEPL (CQ=1). The entanglement generation rate increases proportionally to the number of CQs. SKF is the same value in the case of mEPL (CQ=1) in every case.

	$T_{sg}[s]$	Entanglement generation rate	SKF	SKR
mBK(CQ=1)	3×10^{-5}	1.65	0.559	0.924
mBK(CQ=2)	3×10^{-5}	3.30	0.559	1.85
mBK(CQ=1)	3×10^{-6}	16.2	0.558	9.05
mBK(CQ=2)	3×10^{-6}	32.5	0.558	18.1
mBK(CQ=1)	3×10^{-7}	162	0.558	90.0
mBK(CQ=2)	3×10^{-7}	324	0.558	180

4.3 SUMMARY

- We would like to know how much improvement of the hardware parameter, p_{depsg} , would allow a time-multiplexed protocol to achieve a better SKR than a non time-multiplexed protocol. We find that time-multiplexing in the SC protocol is not useful unless p_{depsg} is improved to be less than 0.002.
- When improving only p_{depsg} or T_{sg} , we would like to know how much SKR can be improved in mEPL and mBK. According to our research, improving T_{sg} is more important in obtaining a better SKR for both protocols.
- When changing the number of CQ from 1 to 2, we would like to know how much SKR can be improved in mEPL and mBK. From our research results, we can see that if T_{sg} is ideally small for both mEPL and mBK, SKR increases proportionally to the number of CQ.

5

EFFECT OF PROTOCOL CHOICE IN SKR ACHIEVABLE BY REPEATER CHAINS WITH LIMITED RESOURCES

In [Chapter 5](#), we will investigate how to distribute resources in order to maximize the SKR in setups of two end nodes connected by up to two repeaters.

5.1 MODELS

In this section, we will explain problem setups for the following research questions:

- What is the best order in which to perform entanglement generation attempts?
- How is the best way to distribute CQs in a chain with two repeaters?

5.1.1 Common settings

For all experiments in [Chapter 5](#), we assume the common hardware parameters shown in [Table 5.1](#) except for the parameters where NV center and trapped ion use different values. For the first research question, we assume NV center parameters. Note that T_{sg} is improved by 99% (or 99.9 %) and p_{depsg} is improved by 99% to get non-zero SKR. For the second research question, we assume that trapped ions are used, since we allow for the possibility that a repeater has more than one communication qubit. We note that the same could be achieved with NV centers by placing multiple diamonds in one node. Besides, T_{sg} is improved by more than 99.9% (or 99.99 %) and p_{depsg} is improved by 99% to get non-zero SKR.

On the other hand, the number of repeaters between end nodes, repeater chain protocol, and the number of CQs (MQs) in the repeaters are different for each research question and will be explained again in each subsection.

With the exception of the above, we employ the same models and calculations for entanglement generation rate and fidelity as explained in [Chapter 4](#) except for the above things. We then start by introducing models for each research question.

5.1.2 What is the best order in which to perform entanglement generation attempts?

Assuming the situation depicted in [Figure 5.1](#) where there is a processing node repeater halfway between Alice and Bob, we want to find which protocol the nodes should employ in order to generate the largest possible end-to-end SKR. In such a case, the ratio of photons emitted by the CQ in the central repeater toward Alice and Bob will affect the SKR. For example, we can think of an extreme case (protocol 1). In protocol 1, we start by sending photons only toward Bob. After it is confirmed that one entangled state between the repeater and Bob has been generated, then photons are sent only toward Alice until entanglement is generated. Finally, an entanglement swap is performed at the repeater and we get end-to-end entanglement. Although the entanglement generation rate between the repeater and each of the end nodes is high, the entangled pair shared by Bob and the repeater will have to

Table 5.1: Common parameter settings in [Chapter 5](#) are listed. Basically, they are based on experimentally realized values. η is the probability that a photon is emitted from each node and reaches the heralding station. p_{fc} is the frequency conversion efficiency from the NV center or the trapped ion wavelength to a telecom fiber. p_{loss} is the probability that a coupling succeeds from the matter to the fiber. N_{max} is the maximum number of MQs that a node can use assuming a number of CQ and an entanglement generation protocol. $T_m(T_c)$ is the coherence time of MQ (CQ). T_{sg} is the swap gate time. p_{depsg} is the probability of introducing depolarizing noise when performing the swap gate. α' is the probability of generating entangled states in [Equation 3.5](#). d is the distance between two end nodes. c is the photon speed in a fiber.

Parameters	NV center	Trapped-ion
η	0.009 [Dam et al., 2017 ; Zaske et al., 2012]	
p_{fc}	0.3 [Zaske et al., 2012]	
p_{loss} [dB/km]	0.2	
N_{max}	depends on entanglement generation protocol	
T_m [s]	1 [Bradley et al., 2019]	0.085 [Krutyanskiy et al., 2022]
T_c [s]	0.5 [Pompili et al., 2021]	0.085 [Krutyanskiy et al., 2022]
T_{sg} [μ s]	2 or 0.2	2 or 0.2
p_{depsg}	0.0017	0.06 [Krutyanskiy et al., 2022]
α'	0.01	
d [km]	100	
c [km/s]	200,000	
Entanglement generation protocol	mSC	

wait a long time before a new entangled state is generated between Alice and the repeater, which will deteriorate SKF.

On the other hand, we can think of another case when photons are alternately sent to Alice and Bob at equal rates (protocol 2). The entanglement generation rate between Alice (Bob) and the repeater is lower compared to the protocol 1, but the time until the second entangled state is generated from the generation of the first entanglement is shorter. Therefore, it is expected to obtain a higher SKF. We would like to investigate which protocol can obtain a larger SKR.

Calculation of secret key fraction between Alice and Bob

Protocol 1

Here, we show how the final state shared between Alice and Bob is derived. We start by generating entanglement between the repeater and Bob by the mSC protocol, which results in the state shown in [Equation 4.6](#). After we know that the first entangled state between the repeater and Bob is generated, we generate the second, between Alice and the repeater which is the same state as [Equation 4.6](#). We set $t = 0$ as the time immediately after which the first state to be successfully entangled is moved to the memory qubit. Therefore, when we assume that the entanglement generation rate between Alice and the repeater is x_a , the entangled state shared by the repeater and Bob when we learn that two entangled states are generated is $\rho_{m_r b m_b}(t = \frac{1}{x_a} + T_{att} - T_{sg})$. The state shared by Alice and the repeater in the same moment is $\rho_{m_a m_r a}(t' = T_{att} - T_{sg})$. We set $t' = 0$ as the time immediately after which the second state to be successfully entangled is moved to the memory qubit. Therefore, when an entangled state is generated between them and the repeater, we get the state of [Equation 5.1](#). $\rho_{m_r a}(\rho_{m_r b})$ represents the state in the MQ that is entangled

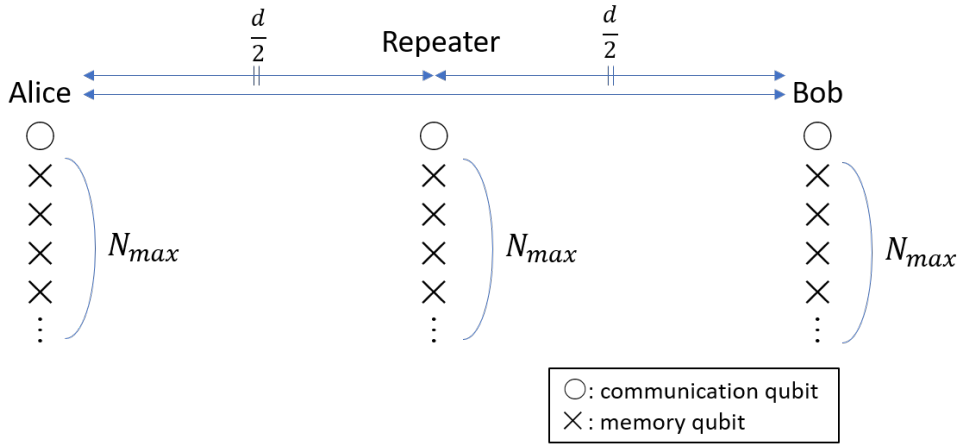


Figure 5.1: Two end nodes (Alice and Bob) are connected by a processing node repeater placed at the halfway point. At each node, there is only one CQ and $N_{max} = \lceil \frac{T_{att}}{T_{sg}} \rceil$ MQs. $T_{att} = d/c$ is 0.25ms

with Alice (Bob) and the repeater. Note that the second state is also moved to a memory qubit, since we use time-multiplexing protocol.

$$\rho_{m_a m_{r_a} m_{r_b} m_b} = \rho_{m_a m_{r_a}}(t' = T_{att} - T_{sg}) \otimes \rho_{m_{r_b} m_b}(t = \frac{1}{x_a} + T_{att} - T_{sg}) \quad (5.1)$$

Then, we perform an entanglement swap as shown in Figure 3.5, with the resulting state being the one given in Equation 5.2. We assume that $U_1 = I_2 \otimes |0\rangle\langle 0| \otimes I_2 \otimes I_2 + I_2 \otimes |1\rangle\langle 1| \otimes X \otimes I_2$ is the CNOT operator using m_{r_b} as the target qubit and m_{r_a} as the control qubit. $U_2 = I_2 \otimes H \otimes I_2 \otimes I_2$ is Hadamard operator on m_{r_a} . Besides, we only assume that the measurement results are always "01" in order to simplify the calculation steps. In other words, we can simply do corrections. Obtaining another measurement outcome would result in identical fidelity, assuming that the correction operations are performed noiselessly. $P_{01} = I_2 \otimes |0\rangle\langle 0| \otimes |1\rangle\langle 1| \otimes I_2$ is the projective operator when the measurement results are "01". Also, $P_i = \text{Tr}[P_{01} \rho_{m_a m_{r_a} m_{r_b} m_b}]$ is the probability that the measurement results are "01".

$$\rho_{m_a m_b} = \text{Tr}_{m_{r_a} m_{r_b}} \left[\frac{P_{01} U_2 U_1 (\rho_{m_a m_{r_a} m_{r_b} m_b}) U_1^+ U_2^+ P_{01}}{P_i} \right] \quad (5.2)$$

Using this state, the quantum bit error rate ($Q_x(Q_z)$) can be calculated by Equation 5.3.

$$\begin{aligned} Q_x &= Pr((x_A = 0 \wedge x_B = 0) \vee (x_A = 1 \wedge x_B = 1)) \\ &= \langle 00 | \rho_{m_a m_b} | 00 \rangle + \langle 11 | \rho_{m_a m_b} | 11 \rangle \\ Q_z &= Pr((x_A = 0 \wedge x_B = 0) \vee (x_A = 1 \wedge x_B = 1)) \\ &= \langle ++ | \rho_{m_a m_b} | ++ \rangle + \langle -- | \rho_{m_a m_b} | -- \rangle \end{aligned} \quad (5.3)$$

The SKF can be calculated by substituting these quantum bit error rates in Equation 2.25.

Protocol 2

We start by generating entanglement between the repeater and Bob (Alice) simultaneously at the same rate by mSC protocol, which results in the state shown in Equation 4.6. Without loss of generality, we assume that an entangled state is generated between the repeater and Bob at first for convenience. Besides, for simplicity,

we assume that each entangled state is generated at almost same time. Since the second entangled state is generated at the next attempt after the first entangled state is generated, the difference between their generation times is T_{sg} . The overall state when an entangled state is generated between them and the repeater results in Equation 5.4. We set $t(t') = 0$ as the time immediately after which the first (second) state to be successfully entangled is moved to the memory qubit.

$$\rho_{m_a m_{ra} m_{rb} m_b} = \rho_{m_a m_{ra}}(t' = T_{att} - T_{sg}) \otimes \rho_{m_{rb} m_b}(t = T_{att}) \quad (5.4)$$

Subsequent steps are identical to protocol 1.

Calculation of entanglement generation rate between Alice and Bob

Protocol 1

The entanglement generation rate between the repeater and Bob, x_b , can be calculated by Equation 5.5 as explained in Chapter 4.

$$x_b = N_{max} \eta \alpha' / T_{att} = \frac{\lceil \frac{(d/2)/c}{T_{sg}} \rceil}{\frac{d/2}{c}} \eta \alpha' \quad (5.5)$$

On the other hand, entanglement generation rate between the repeater and Alice, x_a , can be calculated by Equation 5.6 since an MQ has been already occupied by an entangled state.

$$x_a = (N_{max} - 1) \eta \alpha' / T_{att} = \frac{\lceil \frac{(d/2)/c}{T_{sg}} \rceil - 1}{\frac{d/2}{c}} \eta \alpha' \quad (5.6)$$

Therefore, the entanglement generation rate between Alice and Bob (x_{tot1}) can be calculated by Equation 5.7

$$x_{tot1} = \frac{1}{\frac{1}{x_a} + \frac{1}{x_b}} \quad (5.7)$$

Protocol 2

Since we assume that entanglement between the repeater and each of the end nodes is generated at almost the same time, the entanglement generation rate between Alice and Bob, x_{tot2} , can be calculated by $\frac{1}{\frac{1}{x}} = x$. We assume that $x = 0.5 N_{max} \eta \alpha' / T_{att}$ is the entanglement generation rate between Alice (Bob) and the repeater.

5.1.3 How is the best way to distribute CQs in a chain with two repeaters?

From the results shown in Section 4.2.3, the number of CQs has a big impact on the SKR. However, having access to many CQs per node might be costly. For NVs, it is obvious that it is costly; having multiple CQs would imply having multiple NVs. Therefore, we want to ensure that CQs are distributed in an efficient fashion and obtain large SKR with maximum efficiency.

Assuming the situation as explained in Figure 5.2 where there are two processing node repeaters with the ability to attempt to establish entanglement between Alice and Bob at regular intervals, we want to obtain the largest SKR between Alice and Bob with maximum efficiency. Therefore, we will find the most efficient number of CQs by comparing end-to-end SKRs per CQ for the following three setups.

In setup A (Figure 5.3), there are 2 repeaters, R1 and R2, between Alice and Bob,

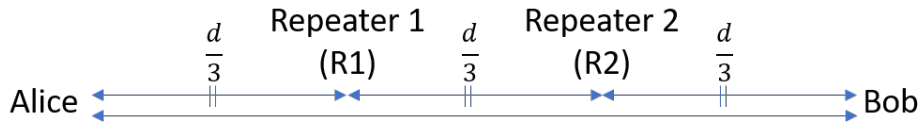


Figure 5.2: There are two processing node repeaters with the ability to emit entangled photons between Alice and Bob at regular intervals. Although a number of CQs is distributed for each node, it should be distributed efficiently because having access to many CQs per node might be costly. Therefore, we want to ensure that CQs are distributed in an efficient fashion and obtain large SKR with maximum efficiency.

and all nodes have only one CQ. As for the number of MQ, we deploy N_{max} , which is the maximum number of MQs that a node can use. Therefore, all nodes have

$$N_{max} = \left\lceil \frac{d/3/c}{T_{sg}} \right\rceil \text{ MQs.}$$

In this situation, we generate entangled pairs between Alice and Bob as follows. We start by generating entanglement between Alice (Bob) and R1 (R2) by mSC. Secondly, when entanglement between them is generated, an entangled pair between R1 and R2 is generated by mSC. Furthermore, an entanglement swap is performed at R1 and R2, and finally an entangled state is generated between Alice and Bob.

In setup B (Figure 5.4), there are 2 repeaters, R1 and R2, between Alice and Bob. Alice and Bob have only one CQ. On the other hand, R1 and R2 have two CQs. As for the number of MQ, we deploy N_{max} , which is the maximum number of MQs that a node can use. In other words, R1 and R2 have $N_{max} = 2 \left\lceil \frac{d/3/c}{T_{sg}} \right\rceil$ MQs. Alice

$$\text{and Bob have } N_{max} = \left\lceil \frac{d/3/c}{T_{sg}} \right\rceil \text{ MQs.}$$

In this situation, we generate entangled pairs between Alice and Bob as follows. We start by generating an entangled pair between all nodes (Alice-R1, R1-R2, R2-Bob) by mSC. Furthermore, when an entangled pair between them is generated, an entanglement swap is performed at R1 and R2, and finally an entangled state is generated between Alice and Bob.

In setup C (Figure 5.5), there are 2 repeaters, R1 and R2, between Alice and Bob, and all nodes have two CQs. As for the number of MQ, we deploy N_{max} , which is the maximum number of MQs that a node can use. In other words, all nodes have

$$N_{max} = 2 \left\lceil \frac{d/3/c}{T_{sg}} \right\rceil \text{ MQs.}$$

In this situation, we generate entangled pairs between Alice and Bob as follows. We start by generating entangled pairs between Alice (Bob) and the R1 (R2) by mSC. Secondly, when entanglement between them is generated, an entangled pair between R1 and R2 is generated by mSC. Furthermore, an entanglement swap is performed at R1 and R2, and finally an entangled state is generated between Alice and Bob. Compared to the setup A, the entanglement generation rate is doubled.

Calculation of secret key fraction between Alice and Bob

Setup A

Here, we show how the final state shared between Alice and Bob is derived. We start by generating entanglement between R1 and Alice, and R2 and Bob by mSC protocol. The resulting state is shown in Equation 4.6. After we know that the first entangled state between both R1 and Alice, and R2 and Bob is generated, we generate the second entangled state between R1 and R2 which is the same state as Equation 4.6. When this state has also been generated, we get the overall state

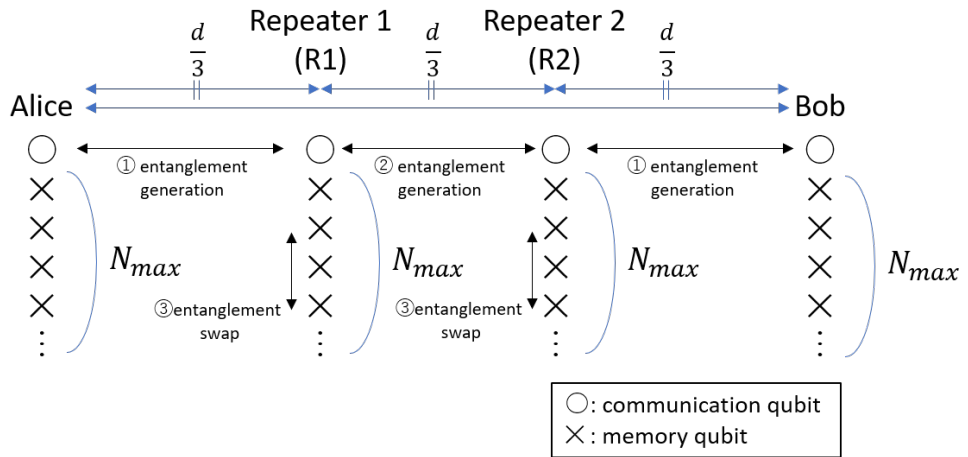


Figure 5.3: Problem setting of setup A. All nodes have only one CQ and $N_{max} = \left\lceil \frac{d/c}{T_{sg}} \right\rceil$ MQs in each repeater. We start by generating entanglement between Alice (Bob) and R1 (R2) by mSC. Secondly, when entanglement between them is generated, an entangled pair between R1 and R2 is generated by mSC. Furthermore, an entanglement swap is performed at R1 and R2, and finally an entangled state is generated between Alice and Bob.

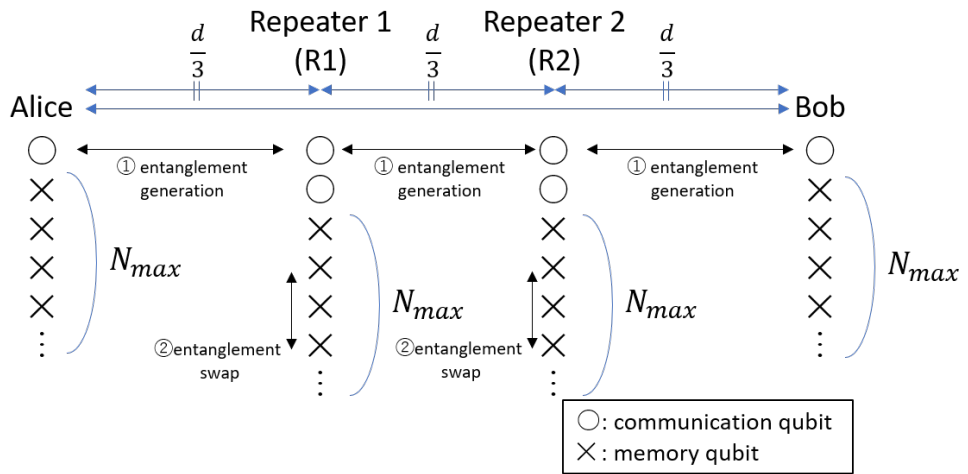


Figure 5.4: Problem setting of setup B. Alice and Bob have only one CQ and $N_{max} = \left\lceil \frac{d/c}{T_{sg}} \right\rceil$ MQs in each repeater. R1 and R2 have two CQs and $N_{max} = 2 \left\lceil \frac{d/c}{T_{sg}} \right\rceil$ MQs in each repeater. We start by generating an entangled pair between all nodes (Alice-R1, R1-R2, R2-Bob) by mSC. Furthermore, when an entangled pair between them is generated, an entanglement swap is performed at R1 and R2, and finally an entangled state is generated between Alice and Bob.

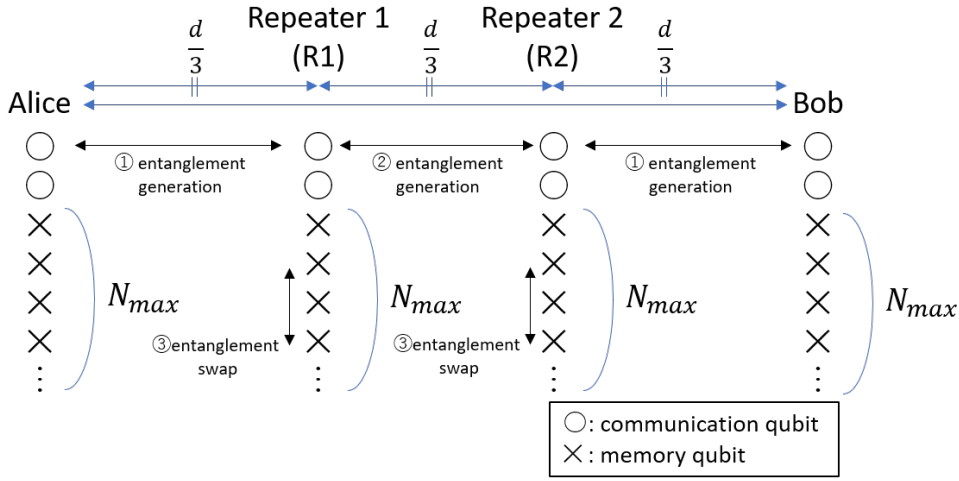


Figure 5.5: Problem setting of setup C. All nodes have two CQs and $N_{\max} = 2 \left\lceil \frac{d/c}{T_{\text{sg}}} \right\rceil$ MQs in each repeater. We start by generating entangled pairs between Alice (Bob) and the R1 (R2) by mSC. Secondly, when entanglement between them is generated, an entangled pair between R1 and R2 is generated by mSC. Furthermore, an entanglement swap is performed at R1 and R2, and finally an entangled state is generated between Alice and Bob.

shown in Equation 5.8.

We set t (t') = 0 as the time immediately after which the first (second) state to be successfully entangled is moved to the memory qubit. In addition, we assume that the entanglement generation rate between R1 and R2 is x_2 . Note that we also assume that the time at which an entangled pair is generated between both R1 and Alice, and R2 and Bob is the same. $\rho_{m_{r1}}(\rho_{m_{r1}'})$ represents the state at R1 which is entangled with the state in MQ at Alice (R2). $\rho_{m_{r2'}}(\rho_{m_{r2}})$ represents the state at R2 which is entangled with the state in MQ at Bob (R1).

$$\begin{aligned}
 & \rho_{m_a m_{r1} m_{r1'} m_{r2} m_{r2'} m_b} \\
 &= \rho_{m_a m_{r1}}(t = \frac{1}{x_2} + T_{\text{att}} - T_{\text{sg}}) \otimes \rho_{m_{r1'} m_{r2}}(t' = T_{\text{att}} - T_{\text{sg}}) \\
 & \otimes \rho_{m_{r2'} m_b}(t = \frac{1}{x_2} + T_{\text{att}} - T_{\text{sg}})
 \end{aligned} \tag{5.8}$$

Then, we perform an entanglement swap as shown in Figure 3.5 at R1 and R2 and the state after performing an entanglement swap at R1 results in Equation 5.9. We assume that $U_3 = I_2 \otimes |0\rangle\langle 0| \otimes I_2 \otimes I_2 \otimes I_2 \otimes I_2 + I_2 \otimes |1\rangle\langle 1| \otimes X \otimes I_2 \otimes I_2 \otimes I_2$ is the CNOT operator using m_{r1}' as the target qubit and m_{r1} as the control qubit. $U_4 = I_2 \otimes H \otimes I_2 \otimes I_2 \otimes I_2 \otimes I_2$ is the Hadamard operator on m_{r1} . Besides, we only assume that the measurement results are always "01" in order to simplify the calculation. In other words, we can simply do corrections. Obtaining another measurement outcome would result in identical fidelity, assuming that the correction operations are performed noiselessly. $P_{01'} = I_2 \otimes |0\rangle\langle 0| \otimes |1\rangle\langle 1| \otimes I_2 \otimes I_2 \otimes I_2$ is the projective operator when the measurement results are "01". Also, $P_{i'} = \text{Tr}[P_{01'} \rho_{m_a m_{r1} m_{r1'} m_{r2} m_{r2'} m_b}]$ is the probability that the measurement results are "01".

$$\rho_{m_a m_{r2} m_{r2'} m_b} = \text{Tr}_{m_{r1} m_{r1}'} \left[\frac{P_{01'} U_4 U_3 (\rho_{m_a m_{r1} m_{r1'} m_{r2} m_{r2'} m_b}) U_3^+ U_4^+ P_{01'}}{P_{i'}} \right] \tag{5.9}$$

Then, the state after performing the entanglement swap at both R1 and R2 results in Equation 5.10. We assume that $U_5 = I_2 \otimes I_2 \otimes I_2 \otimes |0\rangle\langle 0| \otimes I_2 \otimes I_2 + I_2 \otimes I_2 \otimes$

$I_2 \otimes |1\rangle\langle 1| \otimes X \otimes I_2$ is the CNOT operator using $m_{r2'}$ as the target qubit and m_{r2} as the control qubit. $U_6 = I_2 \otimes I_2 \otimes I_2 \otimes H \otimes I_2 \otimes I_2$ is the Hadamard operator on m_{r2} . $P_{01''} = I_2 \otimes I_2 \otimes I_2 \otimes |0\rangle\langle 0| \otimes |1\rangle\langle 1| \otimes I_2$ is the projective operator when the measurement results are "01". Also, $P_{i''} = \text{Tr}[P_{01''}\rho_{m_a m_{r1} m_{r1'} m_{r2} m_{r2'} m_b}]$ is the probability that the measurement results are "01".

$$\rho_{m_a m_b} = \text{Tr}_{m_{r2} m_{r2'}} \left[\frac{P_{01''} U_6 U_5 (\rho_{m_a m_{r2} m_{r2'} m_b}) U_5^+ U_6^+ P_{01''}}{P_{i''}} \right] \quad (5.10)$$

Using this state, the quantum bit error rate ($Q_x(Q_z)$) can be calculated by Equation 5.3. The SKF can be calculated by substituting these quantum bit error rates into Equation 2.25.

Setup B

Here, we show how the final state shared between Alice and Bob is derived. We start by generating entanglement between R1 and Alice, R1 and R2, and R2 and Bob by mSC protocol. The resulting state is shown in Equation 4.6. After we know that the first entangled state between both R1 and Alice, R1 and R2, and R2 and Bob is generated, we get the overall state shown in Equation 5.11.

We set $t = 0$ as the time immediately after which the first state to be successfully entangled is moved to the memory qubit. Note that we also assume that the timing at which entanglement is generated between both R1 and Alice, R1 and R2, and R2 and Bob is same.

$$\begin{aligned} & \rho_{m_a m_{r1} m_{r1'} m_{r2} m_{r2'} m_b} \\ &= \rho_{m_a m_{r1}}(t = T_{att} - T_{sg}) \otimes \rho_{m_{r1'} m_{r2}}(t = T_{att} - T_{sg}) \otimes \rho_{m_{r2'} m_b}(t = T_{att} - T_{sg}) \end{aligned} \quad (5.11)$$

After that, we can calculate the SKF using the same process as setup A.

Setup C

We can calculate SKF using the same process as setup A. But we use $2x_2$ instead of x_2 as entanglement generation rate between R1 and R2.

Calculation of entanglement generation rate between Alice and Bob

Setup A

The entanglement generation rate between Alice (Bob) and R1 (R2), x_1 , can be calculated by Equation 5.5 as explained in Chapter 4. Besides, the entanglement generation rate between R1 and R2, x_2 , can be calculated by Equation 5.6 since an MQ has already been occupied by an entangled state. Note that $N_{max} = \lceil \frac{(d/3)/c}{T_{sg}} \rceil$, and $T_{att} = \frac{3/d}{c}$ in this research question.

Therefore, the entanglement generation rate between Alice and Bob (x_{totA}) can be calculated by Equation 5.7.

Setup B

We assume the entanglement generation rate between R1 and R2, x_B , can be calculated by Equation 5.5 too. Note that $N_{max} = \lceil \frac{(d/3)/c}{T_{sg}} \rceil$, and $T_{att} = \frac{3/d}{c}$ in this research question. Since we assume that the time at which entanglement is generated between both R1 and Alice, R1 and R2, and R2 and Bob is same, the total entanglement generation rate between Alice and Bob, x_{totB} , is also x_B .

Setup C

We can calculate SKF using the same process as setup A. But we use $N_{max} = 2 \lceil \frac{(d/3)/c}{T_{sg}} \rceil$ instead of $N_{max} = \lceil \frac{(d/3)/c}{T_{sg}} \rceil$.

5.2 RESULTS

5.2.1 What is the best order in which to perform entanglement generation attempts?

From [Table 5.2](#), we can see that protocol 1 at $T_{sg} = 2 \times 10^{-6}$ has smaller SKR compared to protocol 2 by 5.90 %. Specifically, protocol 1 has worse SKF and entanglement generation rate compared to the protocol 2. Therefore, when we assume the situation that there is a repeater in the middle of two end nodes, it is better to send photons at the same rate toward the two nodes. After entanglement between Alice (Bob) and the repeater is generated, an entanglement swap is performed at the repeater. If the value of T_{sg} is further improved, the advantage decreases. However, since it is quite difficult to improve T_{sg} by 99.9%, we can still say that protocol 2 has some advantages.

As for the SKF, the value of protocol 1 at $T_{sg} = 2 \times 10^{-6}$ is worse than that of protocol 2 by 5.58 %. This is because $\rho_{m_a m_{ra}}$ in [Equation 5.1](#) and [Equation 5.4](#) are the same state, but for $\rho_{m_{rb} m_b}$, the value of t (t') is $\frac{1}{x_a} - T_{sg}$ larger in protocol 1 than protocol 2. Therefore, the SKF of protocol 1 is worse due to the longer time the state is held in MQ. Incidentally, if the value of T_{sg} is further improved, the difference decreases. This is because T_{att} term in $\rho_{m_{rb} m_b}(t = \frac{1}{x_a} + T_{att} - T_{sg})$ becomes dominant. Actually, we can see this from [Table 5.2](#).

As for the entanglement generation rate, protocol 1 at $T_{sg} = 2 \times 10^{-6}$ is 0.423 % smaller than protocol 2. If T_{sg} is further improved, in other words, N_{max} is further increased, the difference will converge to 0%.

On the other hand, when we consider the case that N_{max} is decreased considering the difficulty of implementing multiple MQs in a node, the advantage of protocol 2 will increase. If N_{max} is smaller, that is, $\frac{1}{x_a} - T_{sg}$ is larger, the SKF of protocol 1 would deteriorate further and the advantage of protocol 2 will increase. As for the entanglement generation rate, the difference between protocol 1 and protocol 2 increases. In other words, the advantage of protocol 2 will increase. This is because the term of “-1” in [Equation 5.6](#) produce greater asymmetry between x_{tot1} and x_{tot2} when N_{max} is smaller. However, we still make sure that this result is biased due to the fact that we consider that entanglement generation between both end nodes succeeds almost simultaneously in protocol 2.

Table 5.2: Results of protocol 1 and protocol 2. When changing the value of T_{sg} , we compare SKF, entanglement generation rate, and SKR between the two protocols. Protocol 1 at $T_{sg} = 2 \times 10^{-6}$ has smaller SKR compared to protocol 2 by 5.90 %. But if the value of T_{sg} is further improved to 2×10^{-7} , the advantage decreases.

	T_{sg} [s]	SKF	Entanglement generation rate	SKR
Protocol 1	2×10^{-6}	0.717	70.9	50.8
Protocol 2	2×10^{-6}	0.757	71.2	53.8
Protocol 1	2×10^{-7}	0.753	711	535
Protocol 2	2×10^{-7}	0.757	712	538

5.2.2 How is the best way to distribute CQs in a chain with two repeaters?

From Table 5.3, we can see that the SKR per CQ is largest in setup B. Therefore, we can say that setup B, in which the number of CQs in a node is equal to that node's number of neighbors, makes best use of its resources. In addition, setup B remains the best even if the value of T_{sg} is further improved.

As for SKF, in setup B entanglement between neighboring nodes is generated simultaneously, which results in shorter waiting time. In other words, entangled states generated between each node do not have to wait for entanglement swap. Therefore, better SKF can be obtained compared to setup C and setup A. In setup A, x_2 is smaller than the one of setup C. Therefore, the entanglement between Alice (Bob) and R1 (R2) gets worse. As a result, SKF of setup A is worse than the one of setup C. Further improving T_{sg} has little effect on the SKF. This is because the state before the entanglement swap, $\rho_{m_a m_{r_1} m_{r_1'} m_{r_2} m_{r_2'} m_b}$, converges to $\rho_{m_a m_{r_1}}(t = T_{att}) \otimes \rho_{m_{r_1'} m_{r_2}}(t' = T_{att}) \otimes \rho_{m_{r_2'} m_b}(t = T_{att})$. Therefore, the ranking of setups according to SKF per CQ is not affected by improvements in T_{sg} .

Regarding the entanglement generation rate, each entanglement generation rate in setup C is twice as fast as the one of setup B. However, setup C needs two steps to generate entangled states between Alice and Bob. As a result, the entanglement generation rate of setup B and setup C is the same. Further improving T_{sg} does not change the relative ordering of the setups.

Table 5.3: Results of setup A, setup B, and setup C. Protocol 1 at $T_{sg} = 2 \times 10^{-6}$ has smaller SKR compared to protocol 2 by 5.90 %. But if the value of T_{sg} is further improved to 2×10^{-7} , the advantage decreases. As for SKF, in setup B, better SKF can be obtained compared to setup C and setup A, since entangled states generated between each node do not have to wait for the entanglement swap. Entanglement generation rate of setup B and setup C is the same. Besides, further improving T_{sg} does not change the relative ordering of the setups.

	T_{sg} [s]	SKF	Entanglement generation rate	SKR	SKR per CQ
Setup A	2×10^{-6}	0.0737	71.3	5.26	1.32
Setup B	2×10^{-6}	0.659	143	94.5	15.8
Setup C	2×10^{-6}	0.319	143	45.5	5.69
Setup A	2×10^{-7}	0.579	712	412	103
Setup B	2×10^{-7}	0.658	1420	937	156
Setup C	2×10^{-7}	0.618	1420	879	110

5.3 SUMMARY

- When considering a situation where there is one repeater in the middle of two nodes, we would like to know what is the best order in which to perform entanglement generation attempts. We find that having the repeater send photons at the same rate towards both end nodes results in a higher SKR than generating entanglement sequentially.
- We would like to know what is the most efficient number of CQ in a protocol with multiple repeaters. We ascertain that the setup B, in which the number of CQs in a node is equal to that node's number of neighbors, makes best use of its resources. Entanglement should be generated in parallel among all nodes.

6 | CONCLUSION

In this section, we summarize all results which are investigated in our research and propose about future works.

6.1 SUMMARY

In this thesis, we investigate how hardware parameters and repeater chain protocols affect the entanglement generation rate and the fidelity by time-multiplexed entanglement generation protocols. As an indicator reflecting both fidelity and entanglement generation rate, the secret key rate (SKR) in quantum key distribution, which has already been commercialized and attracted great public interest, is investigated.

In [Chapter 4](#), we investigate the impact of different hardware parameters on the SKR that can be achieved by two nodes connected without a repeater. Specifically, we examine the following three research questions.

At first, we investigate how much hardware parameter should be improved from an experimentally realized value to achieve a higher SKR using time-multiplexed protocol compared to the non time-multiplexed protocol. From the results in [Section 4.2.1](#), we ascertain that it is not useful to perform time-multiplexing when using a single-click protocol unless p_{depsg} is improved by 98.8 % from the experimentally realized value.

From the previous results, if p_{depsg} is dramatically improved, we know that time-multiplexed protocol can achieve better SKR. However, In addition to p_{depsg} , T_{sg} is also a significant parameter to increase the number of available memory qubits (MQ) and improve SKR in the time-multiplexed protocol. Therefore, in [Section 4.2.2](#), we investigate which hardware parameters are most important for improving SKR. As a result, the improvement of T_{sg} is more important to obtain a higher SKR than the improvement of p_{depsg} .

Besides changing such hardware parameters, SKR can also can be improved by adding extra communication qubits (CQs) in a node. However, in an NV center, there is the limitation that only one communication qubit can be used per an NV center. For example, the trapped ion is a good candidate to use multiple CQs although some hardware parameters' values are worse than the NV center. In [Section 4.2.3](#), we investigate the impact on SKR when changing the number of CQs. Consequently, we ascertain that SKR increases proportionally to the number of CQs under ideal conditions of T_{sg} .

In [Chapter 5](#), we investigate how repeater chain protocols with limited resources, entanglement generation attempt rate in a repeater and the number of CQs, affect SKR and how to optimally distribute the resources to maximize the SKR that can be obtained. We investigate setups with either one or two repeaters. Specifically, we examine the two research questions.

Firstly, when considering a situation where there is one repeater connecting the end nodes, we investigate what the best order is in which to perform entanglement generation attempts in a repeater. From our research results of [Section 5.2.1](#), we find that having the repeater send photons at the same rate towards both end nodes

results in a higher SKR than generating entanglement sequentially.

From the results we got in [Section 4.2.3](#), we know that increasing the number of CQs in a node leads to an increase in the SKR. However, implementing many CQs might be costly. Therefore, secondly, we would like to investigate what is the most efficient number of CQs in a protocol with multiple repeaters. From our research of [Section 5.2.2](#), we ascertain that the setup in which the number of CQs in a node is equal to that node's number of neighbors makes best use of its resources.

6.2 FUTURE WORK

We have found that employing time-multiplexed entanglement generation protocols in devices with experimentally-realized hardware parameters does not lead to an increase in the achievable SKR when compared to non-time-multiplexed protocols. This could be due to several reasons. For example, our research assumes that the swap gate introduces some depolarizing noise, which is the worst-case scenario. Therefore, investigating the case where we use a dephasing noise channel that more accurately represents decoherence and is milder against memory qubits might achieve a larger SKR.

The research also ascertains that dramatic improvements in T_{sg} and the implementation of multiple CQs are key to achieving a larger SKR. However, those dramatic improvements are difficult to achieve immediately. Therefore, it would be interesting to limit the improvement rate of hardware parameters' value and perform the same simulations by improving many parameters gradually instead of improving a single parameter dramatically.

Also, in [Section 5.2.1](#), it is assumed that the repeater is placed in the center of the two nodes. However, this might not be the case. For example, the case where the repeater is placed in an asymmetric position can be possible. Therefore, it is important to conduct a similar investigation for the case.

BIBLIOGRAPHY

- Barrett, S. D. and Kok, P. (2005). Efficient high-fidelity quantum computation using matter qubits and linear optics. *Physical Review A - Atomic, Molecular, and Optical Physics*, 71(6):2–5.
- Bayliss, C. R. and Hardy, B. (2012). Cables 12.1. *Ingenieria electrica de transmision y distribucion*, 4ta edicio:397–466.
- Bennett, C. H. and Brassard, G. (1984). Quantum cryptography: Public key distribution and coin tossing.
- Bennett, C. H., Brassard, G., Crépeau, C., Jozsa, R., Peres, A., and Wootters, W. K. (1993). Teleporting an unknown quantum state via dual classical and Einstein-Podolsky-Rosen channels. *Physical Review Letters*, 70(13):1895–1899.
- Bouwmeester, D. and Zeilinger, A. (2000). *The Physics of Quantum Information: Basic Concepts*.
- Bradley, C. E., Randall, J., Abobeih, M. H., Berrevoets, R. C., Degen, M. J., Bakker, M. A., Markham, M., Twitchen, D. J., and Taminiau, T. H. (2019). A Ten-Qubit Solid-State Spin Register with Quantum Memory up to One Minute. *Physical Review X*, 9(3):31045.
- Branciard, C., Gisin, N., Kraus, B., and Scarani, V. (2005). Security of two quantum cryptography protocols using the same four qubit states. *Physical Review A - Atomic, Molecular, and Optical Physics*, 72(3).
- Chuang, M. N. and I.L. (2011). *Quantum Computation and Quantum Information*, by M.A. Nielsen and I.L. Chuang, volume 52.
- Cirac, J. I., Ekert, A. K., Huelga, S. F., and Macchiavello, C. (1999). Distributed quantum computation over noisy channels. *Physical Review A - Atomic, Molecular, and Optical Physics*, 59(6):4249–4254.
- Collins, O. A., Jenkins, S. D., Kuzmich, A., and Kennedy, T. A. (2007). Multiplexed memory-insensitive quantum repeaters. *Physical Review Letters*, 98(6):98–101.
- Cramer, J., Kalb, N., Rol, M. A., Hensen, B., Blok, M. S., Markham, M., Twitchen, D. J., Hanson, R., and Taminiau, T. H. (2016). Repeated quantum error correction on a continuously encoded qubit by real-time feedback. *Nature Communications*, 7(May):1–7.
- Cuomo, D., Caleffi, M., and Cacciapuoti, A. S. (2020). Towards a distributed quantum computing ecosystem. *IET Quantum Communication*, 1(1):3–8.
- Dam, S. B., Humphreys, P. C., Rozpdek, F., Wehner, S., and Hanson, R. (2017). Multiplexed entanglement generation over quantum networks using multi-qubit nodes. *Quantum Science and Technology*, 2(3).
- D.Kielpinski and Monroe, C. (2002). Architecture for a large-scale ion-trap. *Nature*, 417:709.
- Ekert, A. K. (1992). Quantum Cryptography and Bell’s Theorem. *The American Physical Society*, 67:6.
- Gidney, C. and Ekerå, M. (2021). How to factor 2048 bit RSA integers in 8 hours using 20 million noisy qubits. *Quantum*, 5:1–31.

- Hermans, S. L. N., Pompili, M., Beukers, H. K. C., Baier, S., Borregaard, J., and Hanson, R. (2021). Qubit teleportation between non-neighboring nodes in a quantum network. pages 1–23.
- Horodecki, M., Horodecki, P., and Horodecki, R. (1997). Inseparable two spin- $1/2$ density matrices can be distilled to a singlet form. *Physical Review Letters*, 78(4):574–577.
- Humphreys, P. C., Kalb, N., Morits, J. P., Schouten, R. N., Vermeulen, R. F., Twitchen, D. J., Markham, M., and Hanson, R. (2018). Erratum to: Deterministic delivery of remote entanglement on a quantum network (*Nature*, (2018), 558, 7709, (268–273)), 10.1038/s41586-018-0200-5).
- Jennewein, T., Simon, C., Weihs, G., Weinfurter, H., and Zeilinger, A. (2000). Quantum Cryptography with Entangled Photons. *Physical Review Letters*, 84(20):4.
- Jozsa, R. (1994). Fidelity for mixed quantum states. *Journal of Modern Optics*, 41(12):2315–2323.
- Kalb, N., Reiserer, A. A., Humphreys, P. C., Bakermans, J. J., Kamerling, S. J., Nickerson, N. H., Benjamin, S. C., Twitchen, D. J., Markham, M., and Hanson, R. (2017). Entanglement distillation between solid-state quantum network nodes. *Science*, 356(6341):928–932.
- Krutyanskiy, V., Meraner, M., Schupp, J., Canteri, M., Krcmarsky, V., Bate, J., and Lanyon (2022). No Title. In *Multiqubit Interface for Trapped Ions and Travelling Photons*. American Physical Society.
- Krutyanskiy, V., Meraner, M., Schupp, J., and Lanyon, B. P. (2017). Polarisation-preserving photon frequency conversion from a trapped-ion-compatible wavelength to the telecom C-band. *Applied Physics B: Lasers and Optics*, 123(9):1–9.
- Lily Chen, Stephen Jordan, Y.-K. L. D. M. R. P. (2016). Report on Post-Quantum Cryptography. *Huabei Gongxueyuan Xuebao/Journal of North China Institute of Technology*, 22(3):221–222.
- Malinovsky, V. S., Santra, S., Muralidharan, S., Jiang, L., and Monroe, C. (2019). Quantum repeaters based on two species trapped ions. *Optics InfoBase Conference Papers*, Part F165:0–12.
- Munro, W. J., Harrison, K. A., Stephens, A. M., Devitt, S. J., and Nemoto, K. (2010). From quantum multiplexing to high-performance quantum networking. *Nature Photonics*, 4(11):792–796.
- Muralidharan, S., Li, L., Kim, J., Lütkenhaus, N., Lukin, M. D., and Jiang, L. (2016). Optimal architectures for long distance quantum communication. *Scientific Reports*, 6(February):1–10.
- Pfister, A. D., Salz, M., Hettrich, M., Poschinger, U. G., and Schmidt-Kaler, F. (2016). A quantum repeater node with trapped ions: a realistic case example. *Applied Physics B: Lasers and Optics*, 122(4).
- Pompili, M., Hermans, S. L., Baier, S., Beukers, H. K., Humphreys, P. C., Schouten, R. N., Vermeulen, R. F., Tiggelman, M. J., dos Santos Martins, L., Dirkse, B., Wehner, S., and Hanson, R. (2021). Realization of a multinode quantum network of remote solid-state qubits. *Science*, 372(6539):259–264.
- Rozpdek, F., Yehia, R., Goodenough, K., Ruf, M., Humphreys, P. C., Hanson, R., Wehner, S., and Elkouss, D. (2019). Near-term quantum-repeater experiments with nitrogen-vacancy centers: Overcoming the limitations of direct transmission. *Physical Review A*, 99(5):1–36.

- Sangouard, N., Dubessy, R., and Simon, C. (2009). Quantum repeaters based on single trapped ions. *Physical Review A*, 79(4):1–6.
- Schupp, J., Krcmarsky, V., Krutyanskiy, V., Meraner, M., Northup, T. E., and Lanyon, B. P. (2021). Interface between Trapped-Ion Qubits and Traveling Photons with Close-to-Optimal Efficiency. *PRX Quantum*, 2(2):1.
- Simon, C. and Irvine, W. T. (2003). Robust long-distance entanglement and a loophole-free bell test with ions and photons. *Physical Review Letters*, 91(11):3–6.
- Sinclair, N., Saglamyurek, E., Mallahzadeh, H., Slater, J. A., George, M., Ricken, R., Hedges, M. P., Oblak, D., Simon, C., Sohler, W., and Tittel, W. (2014). Spectral multiplexing for scalable quantum photonics using an atomic frequency comb quantum memory and feed-forward control. *Physical Review Letters*, 113(5):1–5.
- Tanzilli, S., Tittel, W., Halder, M., Alibart, O., Baldi, P., Gisin, N., and Zbinden, H. (2005). A photonic quantum information interface. *Nature*, 437(7055):116–120.
- Wang, Y., Um, M., Zhang, J., An, S., Lyu, M., Zhang, J. N., Duan, L. M., Yum, D., and Kim, K. (2017). Single-qubit quantum memory exceeding ten-minute coherence time. *Nature Photonics*, 11(10):646–650.
- Wootters, W. K. and Zurek, W. H. (1982). A single quantum cannot be cloned. *Nishioka. Y. • Leder. A. & Leder. P. Proc. natn. A cad. Sci. U.S.A*, 299(9):39–42.
- Yuan, Z., Plews, A., Takahashi, R., Doi, K., Tam, W., Sharpe, A. W., Dixon, A. R., Lavelle, E., Dynes, J. F., Murakami, A., Kujiraoka, M., Lucamarini, M., Tanizawa, Y., Sato, H., and Shields, A. J. (2018). 10-Mb / s Quantum Key Distribution. *LIGHTWAVE TECHNOLOGY*, 36(16):3427–3433.
- Zaske, S., Lenhard, A., Keßler, C. A., Kettler, J., Hepp, C., Arend, C., Albrecht, R., Schulz, W. M., Jetter, M., Michler, P., and Becher, C. (2012). Visible-to-telecom quantum frequency conversion of light from a single quantum emitter. *Physical Review Letters*, 109(14):1–5.
- Zhu, Y. M. and Ma, L. (2018). Entanglement distribution in star network based on spin chain in diamond. *Physics Letters, Section A: General, Atomic and Solid State Physics*, 382(25):1651–1655.
- Zwerger, M., Lanyon, B. P., Northup, T. E., Muschik, C. A., Dür, W., and Sangouard, N. (2017). Quantum repeaters based on trapped ions with decoherence-free subspace encoding. *Quantum Science and Technology*, 2(4):1–9.

